In-vitro characterization of pancreatic functional units from Cel-MODY mice

Teresa Hai-Ly Pham

This thesis is submitted in partial fulfilment of the requirements for the degree of Master of Science

Master Thesis

Molecular biology

60 credits

Department of Biological Sciences

Faculty of Mathematics and Natural Sciences

University of Bergen

June 2021

Acknowledgements

The work presented in this thesis has been performed at the Gade Laboratory for Pathology, Department of Clinical Medicine, University of Bergen from August 2020 to May 2021. I have been affiliated with the master program in molecular biology at the Department of Biological Sciences, University of Bergen.

First, I would like to thank my supervisor, Khadija El Jellas, for everything you have taught me during the thesis work. I am truly grateful for all your guidance, all the support and that you were always available to answer all my questions with deep insight into the topics. Our discussions and the work I have done in this interesting project have given me the opportunity to grow as a researcher. Thank you also so much for your positive feedback and all the help during the writing of my thesis.

I would also like to thank my other supervisor, prof. Anders Molven, for giving me the opportunity to be a part of this fantastic research group. I appreciate your knowledge about CEL in particular and research in general. I am also grateful for your support, interesting ideas, and discussions when the experiments did not work as planned and during the writing process.

Moreover, I am thankful to Karianne Fjeld, Anny G. Svanbring, Solrun Steine, Bendik Nordanger and Hege A. Dale. Karianne and Anny, thank you for the valuable information regarding the mice strains. Solrun, thank you for teaching me how to genotype, ordering reagents, and for your kindness. Bendik, thank you for being so helpful with the ordering of reagents and for the processing of the tissues. Hege, thank you for all your technical support at the confocal microscopy.

Furthermore, I would like to thank everyone in the CEL group as well as members of the Center for Diabetes Research; in particular, thanks to prof. Simona Chera and Thomas A. Legøy for sharing protocols and expertise about the islet isolation. I am also very grateful towards colleges at the Pathology Department, special thanks to Stian Tornaas for your good feedbacks; also, to Heidrun Vethe for help when troubleshooting with the islet stimulation experiments. Finally, I would like to thank my family and friends for your cheering and motivation. A special thank you goes to Thor-Narve Mulvik for all encouragement and for always believing in me.

Bergen, June 2021
Teresa Hai-Ly Pham

Abstract

The digestive enzyme carboxyl-ester lipase (CEL) is secreted by pancreatic acinar cells into the duodenum where it hydrolyzes dietary fat, cholesteryl esters, and fat-soluble vitamins. To date, two single-base mutations in the variable number of tandem repeats (VNTR) in the last exon of *CEL* have been identified. These mutations lead to a frameshift and a truncated CEL protein and they cause monogenic diabetes, also known as Maturity-Onset Diabetes of the Young, type 8 (CEL-MODY). In addition to early-onset diabetes, the disease is characterized by the development of multiple cysts and lipomatosis in the pancreas, leading to pancreatic exocrine dysfunction and the progressive deterioration of the pancreas.

To better understand the pathogenic mechanism of CEL-MODY disease, our group has developed a novel mice model. The main objective of this study was to investigate the function of primary acini and islets of Langerhans isolated from Cel-MODY mice. More specifically, we aimed to investigate the viability of primary isolated acini, their secretory capacity, and the intracellular distribution of CEL protein in freshly isolated acini. Furthermore, by testing different protocols for isolating islets of Langerhans from mice pancreas we aimed at characterizing their function by performing glucose-stimulated insulin secretion (GSIS) assays.

Our results revealed no clear differences when performing morphological assessment of cell viability for acini isolated from the different mouse strains. However, measurements of intracellular ATP levels showed significantly lower metabolic rate in acini isolated from Cel-MODY mice compared to control mice. The cellular distribution of CEL-containing granules appeared slightly different for acini isolated from Cel-MODY mice. For this mouse strain, we also observed significant differences in basal secretion of amylase for acini. Isolated islets of Langerhans from MODY8 mice did secrete insulin according to different concentrations of glucose in a similar way as observed in the two control mice strains.

At the histology level, fat infiltration was observed in some pancreatic lobes for 3-month old Cel-MODY mice. Moreover, isolation of acini and islets from this strain resulted in lower amount of cellular material, which possibly could reflect that only acini and isles from intact and healthy lobes of the pancreas survived the isolation procedure and became part of the experiments performed. Investigations of older Cel-MODY (>6 months), where a worse phenotype is expected due to the progressive nature of the pathogenic process, are needed in order to understand better how islet and acini function may be altered in this disease.

Table of contents

Abbreviations

~	Approximately
0/0	Wild type *Cel* alleles (control mice)
0/ki	Heterozygous *Cel* knock-in allele
16R	16 repeat
AP	Acute pancreatitis
ATP	Adenosine triphosphate
bp	Base-pairs
BSA	Bovine serum albumin
CCK	Cholecystokinin
CEL/CEL	Carboxyl-ester lipase gene/protein (human)
Cel/Cel	Carboxyl-ester lipase gene/protein (mouse)
CELP	Carboxyl ester lipase pseudogene
CP	Chronic pancreatitis
DMSO	Dimethyl sulfoxide
ELISA	Enzyme-linked immunosorbent assay
ER	Endoplasmic reticulum
FBS	Fetal bovine serum
GSIS	Glucose-stimulated insulin secretion
H&E	Hematoxylin and eosin staining
HBSS	Hank's Balanced Salt Solution
IF	Immunofluorescence
kb	Kilo bases
kDa	Kilo Daltons
ki/ki	Homozygous knock-in allele
KRB	Krebs buffer
MODY	Maturity-onset diabetes of the young
PBS	Phosphate-buffered saline
PCR	Polymerase chain reaction
PS	Penicillin-Streptomycin
RPMI	Roswell Park Memorial Institute
T1D	Type 1 diabetes
T2D	Type 2 diabetes
TCA	Tricarboxylic acid cycle
VNTR	Variable number of tandem repeats
WT	Wild type

1 Introduction

1.1 The human pancreas

The human pancreas is an elongated gland located behind the stomach (**Figure 1.1 A**) (Reisner, 2014; Smith & Morton, 2010). The organ can be divided into three parts: head, body, and tail (**Figure 1.1 B**). The pancreas and the duodenum are connected by the ampulla of Vater, where the main pancreatic duct and the common bile duct are joined. The main pancreatic duct extends through the whole organ. The pancreas has a bifunctional role since it acts both as an exocrine gland secreting digestive enzymes into the duodenum, and as an endocrine gland secreting hormones into the blood (Frantz et al., 2012; Logsdon & Ji, 2013).

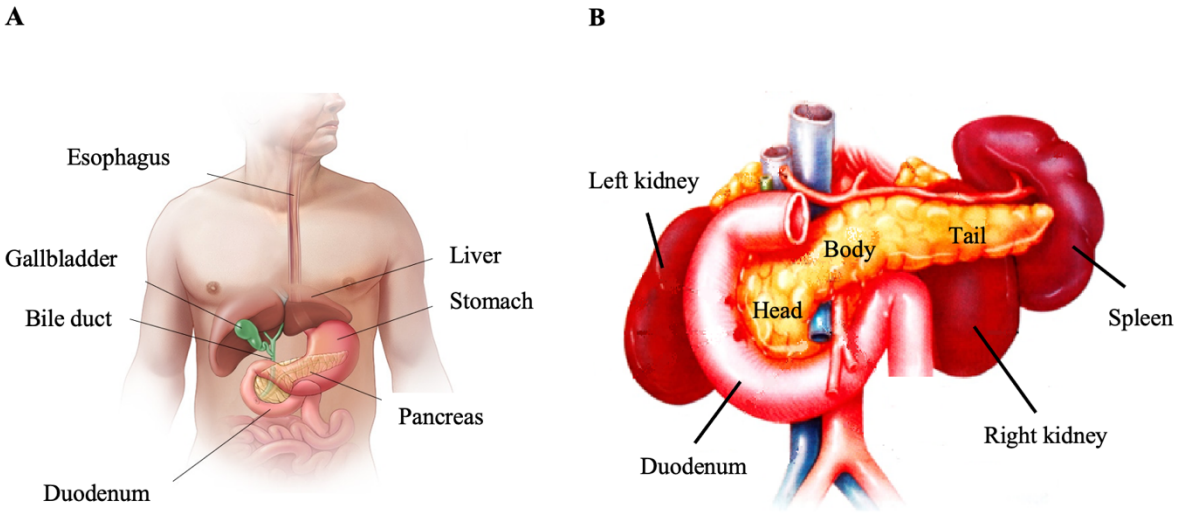

Figure 1.1. **Anatomical overview and relations of the pancreas. A)** The human pancreas is located behind the stomach, extending towards the left part of the upper abdomen. The organ acts both as an exocrine and endocrine gland. Figure from: https://www.mayoclinic.org/diseases-conditions/pancreatic-cancer/symptoms-causes/syc-20355421 **B)** The pancreas is surrounded by the spleen and the kidney on the right side, touching the tail of the pancreas. The head of the pancreas is located in the C-sharped region of the upper curvature of the duodenum. The liver and the gall bladder on the upper right side are not shown. Figure modified from (D. C. Whitcomb & M. E. Lowe, 2007)

1.1.1 The exocrine pancreas

The exocrine part of the pancreas parenchyma represents approximately 90 % of the organ and is comprised of acinar and ductal cells (Pandiri, 2014). The acinar cells are arranged in cell clusters that share a joint lumen and are denoted acini (**Figure 1.2**) (Geron et al., 2014). The acinar lumen is directly connected into the small, intercalated ducts that converge into larger intralobular ducts and finally merge into the main pancreatic duct (Leung & Ip, 2006; Logsdon & Ji, 2013; Longnecker, 2014).

The acinar cells are responsible for producing digestive enzymes such as proteases, amylases, lipases, and nucleases that break down protein, carbohydrates, lipids, and nucleic acids, respectively. The secretion of digestive enzymes matches closely the dietary need (Logsdon & Ji, 2013). These enzymes together with water and bicarbonate make up the pancreatic juice, of which the pancreas can produce 1-2 liters every day (Lee et al., 2002). The pancreas delivers the digestive juice to the duodenum through the ductal system. The contribution from bicarbonate is important and provides an optimal pH environment for the digestive enzymes in the duodenum (Zeng et al., 2018).

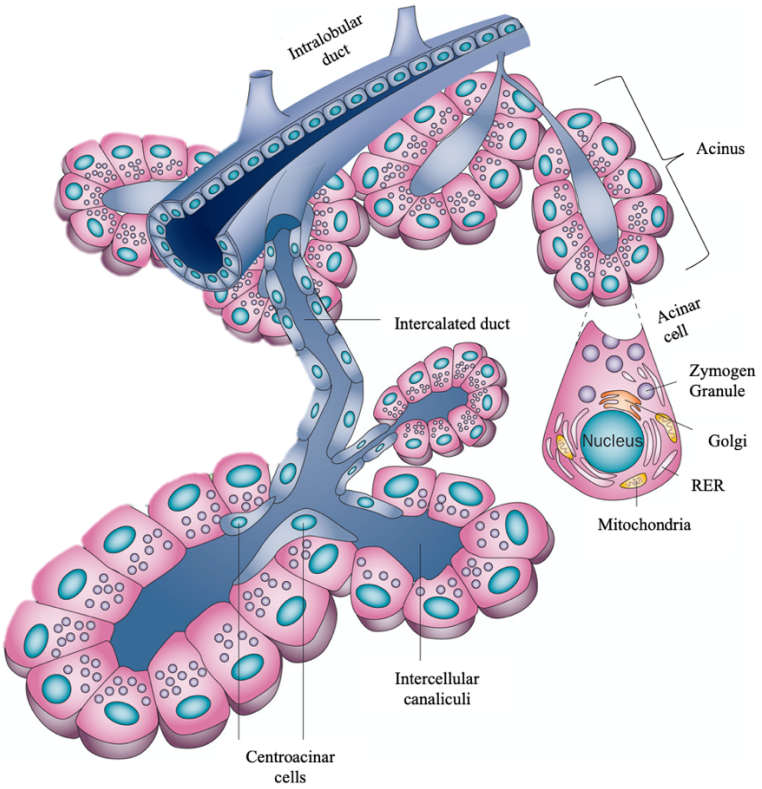

Figure 1.2. **Components of the exocrine pancreas.** Acinar cells surrounding a central lumen are clustered to form an acinus. The acinar cells synthesize, store and secrete digestive enzymes for the digestion and absorption of food in the small intestine. These enzymes are secreted into intercalated ducts that are connected to intralobular ducts, which join into the main pancreatic duct. The latter is connected to the common bile duct right before the ampulla of Vater where the products from the pancreas and the liver enter the duodenum. Figure modified from (Logsdon & Ji, 2013).

The synthesis of the digestive enzymes starts at the ribosomes that are directly attached to the endoplasmic reticulum (ER) membrane (Alberts B, 2002; Leung & Ip, 2006). Thereafter, they are transported to the Golgi network for further processing (Cooper, 2000; Xu & Esko, 2009). Proteins from the ER enter the Golgi apparatus on the cis side and are transported through

cisternae, exiting on the trans side (Cooper, 2000). During transportation, the proteins are modified, sorted, and packed for transport to their designated destinations within the cell via exocytosis (Cooper, 2000). Examples of extensive modification are glycosylation, phosphorylation, proteolysis, and sulfation (Zhang & Wang, 2016). For regulated exocytosis, the pancreatic enzymes have to be sorted and stores in secretory granules (Leung & Ip, 2006).

Secretion of digestive enzymes is primarily induced by hormonal stimulation released during the digestion of food. These hormones are mainly secretin, cholecystokinin (CCK), and gastrin. In addition, there are neural stimuli (Slack, 1995). These stimulations initiate multiple pathways to regulate appropriate amounts of digestive enzymes (Leung & Ip, 2006; Wäsle & Edwardson, 2002). The binding of these secretagogues on the basolateral membrane of the acinar cell leads to various types of signal transduction. In general, CCK is known to activate inositol trisphosphate or diacylglycerol signaling pathways. This results in increased cytosolic Ca^{2+}-concentration and activation of protein kinase C, which stimulates the secretion of digestive enzymes by exocytosis (Williams, 2001; Williams et al., 2002).

1.1.2 The endocrine pancreas

The endocrine part of the pancreas consists of a group of specialized cells known as islets of Langerhans. The islets are surrounded by the pancreatic acini and scattered within the exocrine tissue through the whole parenchyma although they are somewhat more concentrated in the tail (Da Silva Xavier, 2018; Smith & Morton, 2010; Villarreal et al., 2019). Notably, the islets of Langerhans comprise only ~1-2% of the total pancreatic mass (Kim et al., 2019; Rosenthal & Wyre, 2012). The endocrine cells produce different hormones released into the bloodstream and have an important role in regulating glucose homeostasis (Campbell & Newgard, 2021; Ichii et al., 2005; Smith & Morton, 2010). The pancreatic islets differ in both cellular composition and architecture between and within species (Kim et al., 2009; Steiner et al., 2010). The human islets consist of ~ 60 % of insulin-producing β-cells, ~30 % glucagon-producing α-cells, while the remaining ~10 % are made up of somatostatin-producing δ-cells, pancreatic polypeptide-producing γ-cells, and ghrelin-producing ε-cells (**Figure 1.3**) (Brissova et al., 2005; Cabrera et al., 2006; Ichii et al., 2005; Ionescu-Tirgoviste et al., 2015; Orci et al., 1976).

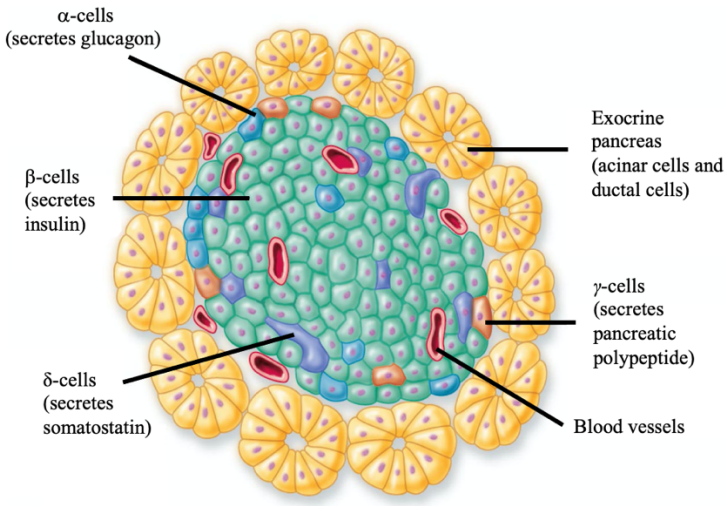

Figure 1.3. **Schematic drawing of an islet of Langerhans.** These islets are groups of specialized cells that secretes hormones into the bloodstream. α-cells, β-cells, δ-cells, γ-cells, and ε-cells that produce glucagon, insulin, somatostatin, pancreatic polypeptide, and ghrelin, respectively. These hormones have an important role in maintaining glucose homeostasis. The ε-cells are not shown in the picture. Figure modified https://ar.pinterest.com/pin/398427898282965328/.

Glucose homeostasis is tightly regulated by the actions of hormones, mainly insulin and glucagon (Campbell & Newgard, 2021; Thorens, 2011). Secretion of these hormones is controlled by different regulatory mechanisms and is essential for the control of glucose levels in the blood (Campbell & Newgard, 2021). The β-cells produce inulin typically after a meal when the blood glucose levels rise. Insulin is secreted into the bloodstream and stimulates uptake and storage of glucose in peripheral tissues such as the liver, skeletal muscle, and adipose tissue to prevent hyperglycemia (Campbell & Newgard, 2021). In contrast to insulin, glucagon is the counter-hormone to insulin and is typically produced in the fasting state (Da Silva Xavier, 2018). When the blood glucose levels drop, α-cells produce glucagon to raise fatty acids and glucose concentration in the bloodstream and the major function is to prevent hypoglycemia (Gerich, 1988; Gerich & Campbell, 1988). The balance between insulin and glucagon helps the cells to have efficient energy, but also preventing damage that can result after high levels of blood sugar over a period (Kalra & Gupta, 2016).

The secretion of insulin is a complex process, and some knowledge about it is necessary for understanding diabetes mellitus (see section 1.2.1). Increased glucose concentration stimulates insulin secretion, referred to as glucose-stimulated insulin secretion (GSIS). The pancreatic β-

cells take up the glucose via GLUT1 (human) or GLUT2 (rodents) transporters. Following phosphorylation by glucokinase (GK), which controls the entrance of glucose into the glycolytic pathway, glucose is converted to pyruvate. It them enters the tricarboxylic acid (TCA) cycle to subsequently generate adenosine triphosphate (ATP). This causes closure of K_{ATP} channels and plasma membrane depolarization. Once membrane depolarization occurs, voltage-gated calcium channels (VGCC) opens and increases Ca2+ concentration in cells. This results in increased intracellular calcium drivers that trigger insulin granule exocytosis and activate insulin secretion (**Figure 1.4**) (Campbell & Newgard, 2021; Castiello et al., 2015; Girgis & Gunton, 2012).

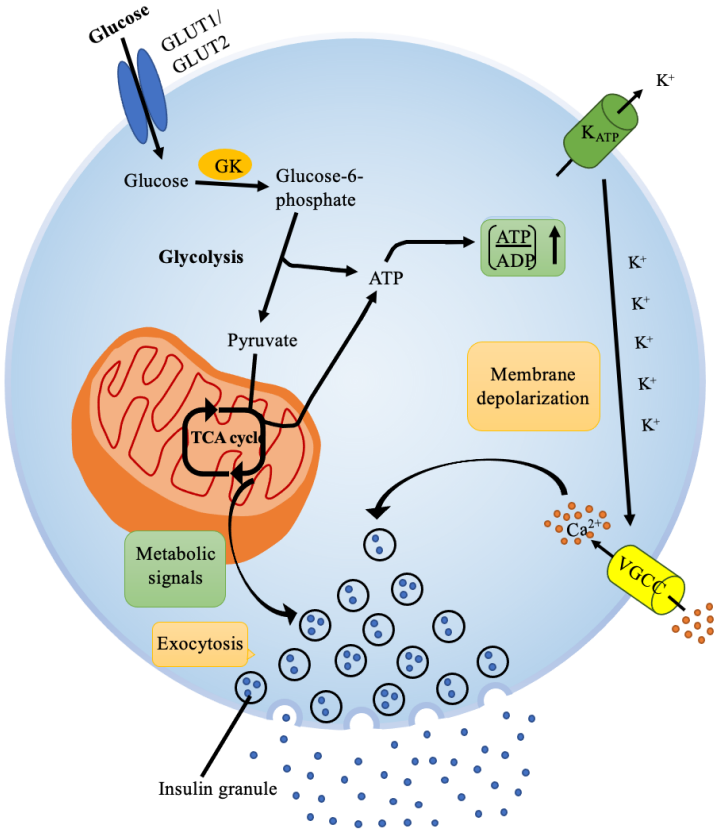

Figure 1.4. **Steps involved in glucose-stimulated insulin secretion (GSIS) by pancreatic β-cells**. Glucose enters the cell via GLUT1 or GLUT2 transporters for humans and rodents, respectively. Glucokinase (GK) phosphorylates glucose and serves as an important regulation step. Pyruvate is formed by the process of glycolysis. This causes increased activity of the TCA cycle and production of adenosine triphosphate (ATP). ATP molecules bind to the K_{ATP} channels resulting in channel closure, depolarization of the plasma membrane, and activation of voltage-gated calcium channels. Calcium enters the cell and triggers insulin granules to be released into the circulation. Figure modified from (Campbell & Newgard, 2021).

1.2 Pancreatic diseases

1.2.1 Diabetes mellitus

Diabetes mellitus is a metabolic disorder characterized by chronically raised levels of glucose in the blood (hyperglycemia) (Asmat et al., 2016). The disease results from a deficiency in the production, secretion, or action of insulin (Maritim et al., 2003). Diabetes mellitus is often classified as either type 1 diabetes (T1D) or type 2 diabetes (T2D). However, there are other forms such as gestational diabetes and maturity-onset diabetes of the young (MODY).

Type 1 diabetes (T1D) is an autoimmune disease where immune cells attack and destroy the insulin-producing β-cells and cause deficiency of insulin secretion (American Diabetes, 2010). Historically, T1D was the type of diabetes observed in children and teenagers, but over the past decades, this view has changed. Age at the symptomatic outbreak is no longer a limiting factor for the diagnosis of T1D (Atkinson et al., 2014; Leslie, 2010) although it is still one of the most common chronic diseases of youth (Gale, 2005). Patients with T1D require exogenous insulin replacement and need the treatment throughout life (Atkinson et al., 2014).

Over the last decade, the global increase in obesity, unhealthy diet, physically inactive lifestyle, and an aging population has quadrupled the number of patients with Type 2 diabetes (T2D) (DeFronzo et al., 2015; Zhou et al., 2016). T2D represents more than 90 % of all diabetes cases (Chatterjee et al., 2017), and is characterized by insulin deficiency caused by dysfunction of the β-cells and/or resistance of insulin action in target organs (Chatterjee et al., 2017). Increased gluconeogenesis is considered a crucial contributor to hyperglycemia (Hatting et al., 2018; Magnusson et al., 1992).

Monogenic diabetes accounts for 1-2 % of all diabetes cases (Kleinberger et al., 2018) and results from a mutation in a single gene (Broome et al., 2021). Maturity-onset diabetes of the young (MODY) is the most common type of monogenic diabetes (Broome et al., 2021). MODY is traditionally associated with an autosomal dominant pattern of inheritance (Vaxillaire et al., 1995) and β-cell dysfunction (Gardner & Tai, 2012; Peixoto-Barbosa et al., 2020). The disease typically presents before 25 years of age. MODY is heterogeneous genetically, and it is thought to account for ~1-2 % of all diabetes cases (Gardner & Tai, 2012; Vaxillaire et al., 1995). However, the disease is often misdiagnosed as T1D or T2D (Gardner & Tai, 2012). To date, 14 subtypes of MODY are identified (Anık et al., 2015; Fajans et al., 2001; Firdous et al., 2018;

Oliveira et al., 2020; Urakami, 2019). The most common subtypes are mutations in genes associated with glucokinase and hepatocyte nuclear factors (HNFs) (Nkonge et al., 2020).

1.2.2 Pancreatic cancer

Pancreatic cancer is a disease with high mortality and associated with a bad prognosis (Siegel et al., 2014). Most patients do not have symptoms until the disease reaches an advanced stage. Globally, pancreatic cancer is the ranks as the seventh highest cause related to cancer death in the world, while in the United States it is the fourth highest (Rahib et al., 2014; Rawla et al., 2019).

Pancreatic cancer can arise from both endocrine and exocrine tissues. However, the most common pancreatic neoplasm is pancreatic ductal adenocarcinoma (PDAC). PDAC develops in the exocrine tissues and constitutes more than 90 % of pancreatic cancer cases (Sarantis et al., 2020). The major risk factors associated with pancreatic cancer are cigarette smoking, diabetes mellitus, chronic pancreatitis, age, and family history of the disease (Kamisawa et al., 2016). Around 70 % of PDAC cases arise from the head of the pancreas and are usually diagnosed earlier than tumors appearing in the body and tail (Corbo et al., 2012). Common symptoms observed in patients are abdominal pain, jaundice, and weight loss (Porta et al., 2005).

1.2.3 Pancreatitis

The physiological functions of exocrine acinar cells are to produce, store, and secrete digestive enzymes. Disorders of these cells and functions often lead to the pathologic inflammation of the pancreas known as pancreatitis (Bläuer et al., 2014; Leung & Ip, 2006). Inappropriate release and activation of trypsinogen to trypsin within the acini triggers the activation pathway of different digestive enzymes resulting in autodigestion of the organ (Mederos et al., 2021; Roxvall et al., 1991; Uehara et al., 1989). Acute pancreatitis is an acute inflammation of the pancreas that arises within a short period of time and can go away after some few days of treatment, eventually leaving the pancreas healed (Ahmed Ali et al., 2016). In some cases, repeated attacks of acute pancreatitis eventually progress to chronic pancreatitis where there is permanent damage to the organ (Ahmed Ali et al., 2016).

Acute pancreatitis (AP) is a complex disease with variable severity; some patients have mild attacks while others suffered severe and highly morbid attacks (Bhatia et al., 2005). Leading causes of AP are gallstone disease and alcohol. However, other causes include infection, genetic predisposition and trauma (Mederos et al., 2021). Following acute pancreatitis, one of five patients gets diabetes, and exocrine pancreatic insufficiency as a complication (Lee & Papachristou, 2019). Many AP patients have reduced long-term quality of life and many have frequent hospitalizations (Lee & Papachristou, 2019).

Chronic pancreatitis (CP) is a progressive fibroinflammatory syndrome where repetitive pancreatic inflammation incidents lead to persistent pathological responses to injury or stress in the pancreas (Beyer et al., 2020; Kleeff et al., 2017). CP is characterized by continued inflammation in the pancreas that results in loss of the exocrine and endocrine tissue because of atrophy and/or extensive replacement by fibrotic tissue (Beyer et al., 2020; Kleeff et al., 2017). Structural changes of the pancreas result in permanent damage and insufficiency in both exocrine (diabetes mellitus) and endocrine functions (maldigestion) (Beyer et al., 2020; Kleeff et al., 2017). The pathophysiology of CP includes injury in the acinar cell, acinar stress responses, dysfunction of the pancreatic ducts, and persistent or altered inflammation (Kleeff et al., 2017). CP also increases the risk factor for subsequent pancreatic cancer (Kirkegård et al., 2017).

1.3 Carboxyl-ester lipase (CEL)

Carboxyl ester lipase (CEL) is a digestive enzyme secreted by the acinar cells of the pancreas. The enzyme is secreted in a partly inactive form to the duodenum, where it is fully activated by bile salts (Bläckberg et al., 1981; Hui & Howles, 2002; David C. Whitcomb & Mark E. Lowe, 2007). Therefore, the enzyme is also referred to as bile salt-stimulated/dependent lipase (BSSL/BSDL) (Abouakil & Lombardo, 1989; Hernell & Olivecrona, 1974). Activated CEL can hydrolyze dietary fat, cholesteryl esters, and fat-soluble vitamins (Bläckberg & Hernell, 1983; Hui & Howles, 2002; Lombardo et al., 1978; Lombardo & Guy, 1980). CEL is one of four lipases secreted by the exocrine pancreas and the protein is estimated to represent ~4 % of the total proteins detected in the pancreatic juice (Lombardo et al., 1978). CEL is also abundantly expressed in the lactating mammary gland and comprises ~1-2 % of total proteins in the mother's milk (Bläckberg et al., 1981; Johansson et al., 2018).

1.3.1 The human *CEL* locus

The human *CEL* gene is ~10 kb in size and located on chromosome 9q34.13 (Lidberg et al., 1992; Taylor et al., 1991). The gene consist of 11 exons and the last exon includes a GC-rich variable number of tandem repeat (VNTR) region. The VNTR is built of almost identical segments of 33 bp that code for 11 amino acids each.

The CEL gene is very polymorphic due to the VNTR. In humans, from 3 to 23 repeats have been observed, but 16 repeats are the most common allele found in the human population (Bengtsson-Ellmark et al., 2004; Ræder et al., 2006; Torsvik et al., 2009). Eleven kb downstream for the CEL gene is the CEL pseudogene (CELP) located (**Figure 1.5**) (Lidberg et al., 1992; Madeyski et al., 1998). The CELP gene lacks exons 2-7 compared to the CEL gene and is not expected to be translated into any functional protein due to the truncated protein and the presence of a stop codons within the reading frame (Nilsson et al., 1993). CEL and CELP have high sequence homology and share 97 % sequence similarity (Madeyski et al., 1998).

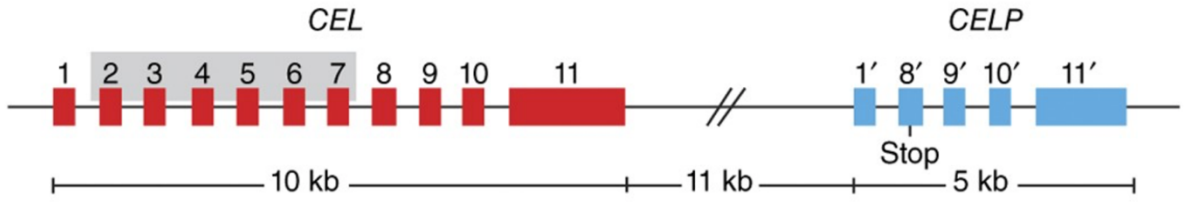

Figure 1.5. **Illustration of the human *CEL* locus.** The *CEL* gene (red) spans ~10 kb and consists of 11 exons. Eleven kb downstream of the *CEL* gene are a pseudogene (CELP) is located (blue). CELP is lacking exon 2-7 of the *CEL* gene (gray shading) and contains a stop codon in exon 8'. The locus is located at chromosome 9q34.13. Figure from (Fjeld et al., 2015).

1.3.2 The CEL protein

CEL contains two different structural domains: An N-terminal globular domain followed by a C-terminal sequence. The N-terminal is a catalytic domain containing the catalytic site, multiple binding sites for bile salts, and a signal peptide (**Figure 1.6**) (Johansson et al., 2018). The C-terminal contains a VNTR region enrich in proline (P), glutamic acid (E), serine (S), and threonine (T) (PEST sequence) (Rogers et al., 1986). The CEL protein is N-glycosylated by the endoplasmic reticulum (ER) at residue Asn187 with help of glucose-regulated protein 94 (GRP94). This modification is important for correct folding and secretion of CEL (Abouakil et al., 1993).

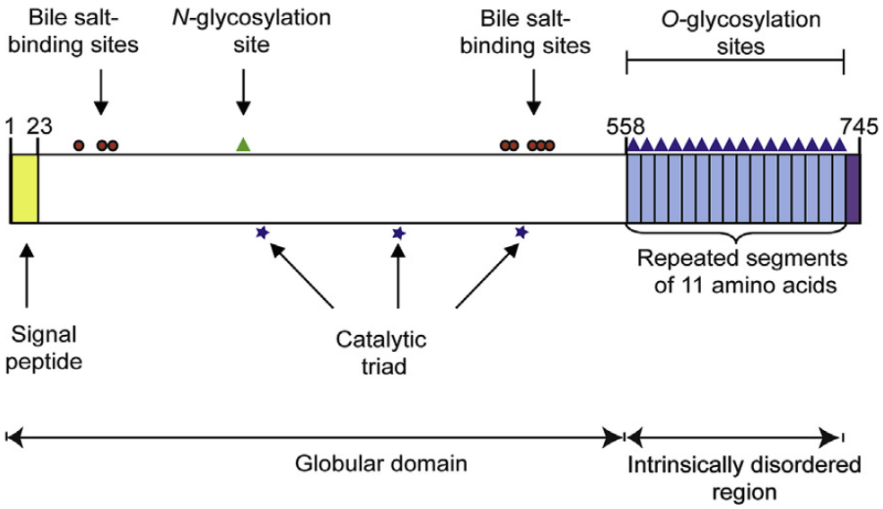

Figure 1.6. **Schematic overview of the structural domains of the CEL protein.** The protein contains two functional domains: A globular N-terminal catalytic domain and an intrinsically disordered C-terminal domain. Signal peptide, bile salt-binding sites, N- and O-glycosylation site, and the catalytic triad are indicated by arrows in the figure. The protein presented contains 16 VNTR repeats, corresponding to the most common variant. The numbers refer to the position of amino acids. Figure from (Johansson et al., 2018).

Thereafter, *CEL* is transported to the Golgi where it is heavily O-glycosylated at the serine and threonine residues of the PEST sequences in the C-terminus (Bruneau et al., 1997; Loomes et al., 1999). It has been suggested that O-glycosylation is important for protecting against protein degradation by masking the PEST sequences (Rogers et al., 1986). After glycosylation, CEL is phosphorylated at residue Thr340 allowing translocation through the secretory pathway, and the protein is stored into zymogen granules with other digestive enzymes (Pasqualini et al., 2000). The CEL variant with 16 VNTR repeats has a predicted molecular mass of ~79 kDa (Johansson et al., 2018), but the size is higher due to the N- and O-glycosylation and can weigh up to 120 kDa (El Jellas et al., 2018).

1.4 Pathogenic variants of CEL

1.4.1 The CEL-MODY variants

CEL-MODY, also known as MODY8 is caused by mutations in the CEL VNTR. CEL-MODY is characterized by progressing pancreatic exocrine dysfunction in addition to lipomatosis and cyst development (Johansson et al., 2011; Ræder et al., 2007; Ræder et al., 2014; Torsvik et al., 2014). The disease has an autosomal dominant pattern of inherence (Johansson et al., 2011).

CEL-MODY has been discovered as different single-base deletions in two Norwegian families (Ræder et al., 2006; Torsvik et al., 2009). These deletions have been located in the first repeat (DEL1) and fourth (DEL4) of the CEL VNTR (Torsvik et al., 2009). Both mutations result in a frameshift and premature stop codon, so the CEL-MODY variants encode for truncated proteins. The aberrant protein carries a different and shorter C-terminal, which is still repetitive with a reduced number of potential O-glycosylation sites (Ræder et al., 2006). In addition, to Norwegian families, additional CEL-MODY cases have been recently discovered in a family from Sweden, Czech Republic, and one from Italy has been discovered (El Jellas et al., 2021; Pellegrini et al., 2021).

Some studies show that the CEL-MODY protein has an increased tendency to aggregate intra- and extracellularly. These aggregates induce ER-stress and cause apoptosis (Gravdal et al., 2021; Johansson et al., 2011; Torsvik et al., 2009; Xiao et al., 2016). Due to inappropriate disulfide bridges, CEL-MODY most likely forms insoluble aggregates. These aggregates are the results of ER stress and activation of the unfolded protein response and most likely they trigger apoptosis (Gravdal et al., 2021; Xiao et al., 2016).

1.4.2 The CEL-HYB variants

Our group has identified a hybrid allele (CEL-HYB), which is a genetic risk factor for chronic pancreatitis (Fjeld et al., 2015). The deletion hybrid variant is probably a result of non-allelic homologous recombination, a crossover between the *CEL* gene and the pseudogene *CELP*. CEL-HYB contains exon 1-10 from the *CEL* gene and exon 11 of the pseudogene (Fjeld et al., 2015). Non-allelic homologous recombination is a common biological mechanism initiated by double-strand breaks in the chromosomes and it generates rearrangements in the genome (Hurles & Lupski, 2006; Parks et al., 2015). This homologous recombination usually happens between two genes that share a high sequence similarity (Beckmann et al., 2007; Colnaghi et al., 2011; Hurles & Lupski, 2006). As mentioned, the genomic sequence of *CEL* and *CELP* have a high sequence similarity (Fjeld et al., 2015). The CEL-HYB allele gives rise to a CEL enzyme with a truncated tail, due to the stop codon in repeat 2 in the CELP VNTR. This results in a lower enzymatic activity than the normal WT protein (Fjeld et al., 2015).

1.5 Established animal models for chronic pancreatitis

Well-characterized animal models are important for investigations that allow translation of experimental results to human conditions. There are many existing experimental models for studying chronic pancreatitis such as the duct-obstructive model (Hyun & Lee, 2014), repetitive overstimulation with cerulein (Lampel & Kern, 1977; Saluja et al., 1985), and chronic alcohol feeding (Lerch & Gorelick, 2013),. In addition, several genetic models have been generated that mimic features of chronic pancreatitis in humans (Aghdassi et al., 2011; Hyun & Lee, 2014; Jancsó & Sahin-Tóth, 2020).

The duct-obstructive model, which relies on surgical ligation of the pancreatic duct, can be used for the introduction of pancreatic fibrosis. Duct obstruction in rats results in fibrosis and acinar cell atrophy without an intensive inflammatory reaction (Hyun & Lee, 2014). The mouse pancreas is, however, made up of three different lobes that drain the pancreatic secretions into individual ducts (Lambert, 1965). This, along with the smaller size, makes duct obstruction more challenging to perform in this small animal model (Hyun & Lee, 2014).

A widely used experimental animal model for chronic pancreatitis is induction by cerulein (Lampel & Kern, 1977; Saluja et al., 1985). Cerulein is a synthetic analogue of CCK (Levy, 2009) and known to induce activation of pancreatic enzymes by intravenous or intraperitoneal injection of this substance in mice, resulting in collagen deposits and fibrosis (Lampel & Kern, 1977; Saluja et al., 1985; Yamamoto et al., 2006).

Alcohol is one of the major risk factors of CP. Chronic alcohol administration can induce pancreatitis. Alcohol alone does not induce CP in rodents, even at a longer experimental time (Lerch & Gorelick, 2013). However, the combination of alcohol and agents such as cerulein worsens pancreatitis and results in fibrosis and a reduction of acinar cell mass (Neuschwander-Tetri et al., 2000).

Genetic analyses can identify specific factors that are associated with pancreatitis. Some genetic models might help to understand the development of pancreatitis. One example is the trypsinogen hereditary model. Premature trypsinogen activation is an important event in the early phases of pancreatitis, and mutations in the trypsinogen gene and its inhibitors might play a role here (Aghdassi et al., 2011). Several studies have overexpressed the human or rodent *PRSS1* gene or inserted a mutated *PRSS1* transgene that leads to trypsinogen autoactivation

(Archer et al., 2006; Athwal et al., 2014; Gaiser et al., 2011). This results in pancreatic inflammation, fibrosis, and fatty infiltration. However, the expression of human *PRSS1* has recently been reported to be toxic to the mouse pancreas, which is a limitation of this model (Hegyi & Sahin-Tóth, 2017).

1.6 Genetically engineered mice (GEM) models for human disease

Creating mouse models by genetic engineering is a powerful tool for studying the cellular pathways and molecular mechanisms of human diseases (Doyle et al., 2012). Genetically modified mice in which the genome has been altered by introducing foreign DNA, are known as transgenic mice (Doyle et al., 2012). The ability to delete, insert or replace DNA in a genome can cause loss-of-function or gain-of-function phenotypes, or can modify the expression of specific genes (Doyle et al., 2012). The most common GEM type is denoted knock-out (KO) and involves removal or inactivation of a specific gene. Alternatively, the gene's activity may be inhibited (Narasimhan et al., 2016). In knock-in (KI), models, the desired gene or gene fragment is inserted or replaced at a specific locus with the intention to express the externally supplied gene (Raz & Perouansky, 2019).

1.6.1 Generating knock-in (KI) transgenic mice by homologous recombination

Gene targeting allows the introduction of mutations at a pre-determined locus of the mouse genome. Construction of KI mice can be archived by homologous recombination and can be performed in murine embryonic stem (ES) cells through a stable transfection such as electroporation or microinjection of the target vector (Hall et al., 2009). The target vector contains the recombinant DNA sequence of interest and a positive selection marker. A positive selection marker is required to enhance clones that contain the targeting vector since the transformation efficiency is low (Ledermann, 2000). The most common drug used for positive selection is neomycin, where the neomycin phosphotransferase gene provides resistance to neomycin (Hall et al., 2009). The positive drug selection marker and the DNA of interest are flanked by two homology arms. These homology arms will be recognized by the endogenous DNA repair machinery, a mechanism for repairing DNA double-stranded breaks, direct error-free repair, and generated variation in the sequence during meiosis (Li & Heyer, 2008). The drug resistance permits the positive selection of the recombinant embryonic stem cells after the homologous recombination. A negative selection marker can be placed adjacent to one of the

targeting arms, that generate a toxic compound when the homologous recombination has not taken place (Hall et al., 2009).

The recombinant ES cells are then injected into mouse blastocysts where they can differentiate into any cell types or tissues (Condic, 2014; Hall et al., 2009). The blastocysts are implanted into female mice made pseudopregnant by hormone treatment. Pseudopregnancy resembles pregnancy except that there is no fetus in the uterus (Murphy, 2018). The offspring will then originate from different mouse strains and some of the mice will be chimeric. The chimeric mice are composed both of normal cells and genetically manipulated cells and will have different coat colors (Eckardt et al., 2011). The chimeric mouse can be transmitted to the next generation to check if the genetic change is in the germline. Further, the chimeric pups can be used for breeding with Cre expressing mice. The recombinase Cre can recognize the loxP flanked by the positive selection marker and cut it out (Hall et al., 2009). By this method, it is possible to generate heterozygous mice for the recombinant DNA in the next generation. An overview of steps involving generating transgenic mice is depicted in **Figure 1.7**.

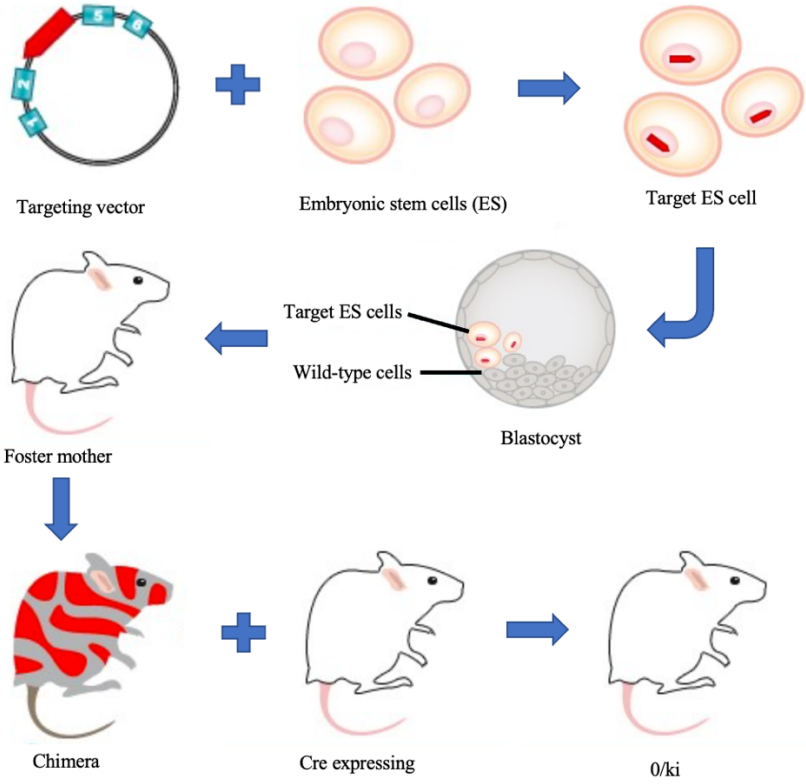

Figure 1.7. **Overview of generating transgenic mice by homologous recombination**. The target vector contains an exogenous sequence (red box) and homology arms (blue boxes) and is transfected into embryonic stem cells (ES). Selection markers permit positive and negative selection of the recombinant embryonic stem cells after the homologous recombination. The blastocyst containing the target ES cells and wild-type cells are implanted into

the foster mother by making a pseudopregnancy. The foster mother will give birth to chimeric pups that need to be bred to check for germ-line transmission of the transgene. The chimeric pups are bred with Cre expressing mice to remove the selection marker in the exogenous sequence. The offspring are heterozygous for the exogenous sequence, marked as 0/ki. Figure modified from GenOway report.

1.6.2 Construction of Cel-MODY and Cel-16R transgenic mice

To study the etiology of CEL-MODY at the organ level, our group has developed a mouse model for the disease. The construction of the transgenic mouse model was similar to the techniques described in section 1.6.1.

The main difference between the CEL protein to mouse and humans is that mouse CEL has 3 VNTR repeats, while in humans has from 3 to 23 VNTR repeats with 16 repeats being the most common in the general population. Cel-MODY humanized mouse model has substituted the normal WT mice VNTR with the mutated VNTR from the first identified Norwegian family. The mutation is localized in the first repeat in a 14 VNTR repeat allele (Ræder et al., 2006).

In addition to Cel-MODY model, a humanized mouse model with 16 normal VNTR repeats (Cel-16R) was developed to generate a control line that expressed the WT form of VNTR. The motivation for using Cel-16R strain is to have a separate control to observe any potential phenotype differentiation due to the partial humanization from a phenotype linked to the mutation. The WT mouse Cel gene and developed humanized Cel-MODY and Cel-16R mice are presented in **Figure 1.8**.

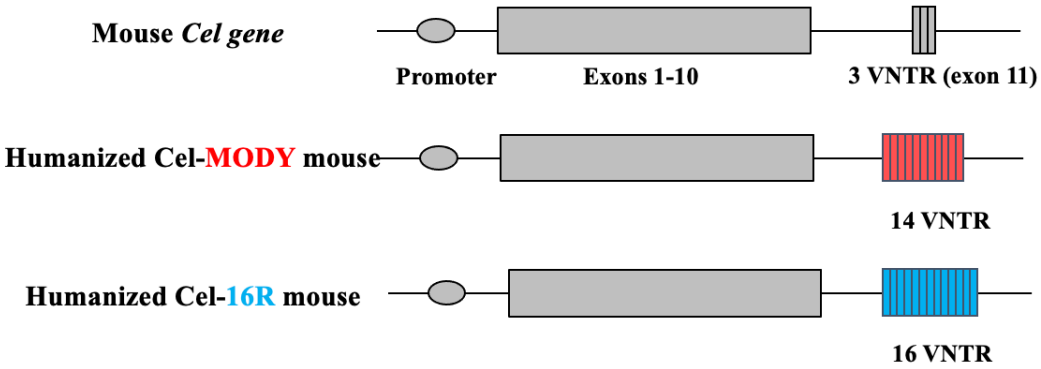

Figure 1.8. **Schematic representation of the WT mouse Cel gene together with humanized Cel-MODY and Cel-16R knock-in gene.** The gene contains a promoter and 11 exons with a VNTR region located in the last exon. The normal WT Cel gene contains 3 VNTR repeats while transgenic Cel-MODY contains 14 human VNTR repeats with a mutation in the first repeat. The latter VNTR is indicated by red boxes. Humanized Cel-16R mouse has the human CEL VNTR with 16 repeats instead the mouse VNTR, indicated as blue boxes.

2 Aims of the study

The overall aim of the project was to investigate the pathogenic mechanisms of the human disease CEL-MODY by studying acini and islets of Langerhans freshly isolated from Cel-MODY mice.

The specific aims were:

1) To establish isolation and separation protocols of acinar cells and islets of Langerhans from mice pancreas
2) To characterize the function of freshly isolated acini from Cel-MODY mice by
    a. Examining cell viability
    b. Determining their secretory capacity upon stimulation with secretagogue
    c. Investigating the intracellular distribution of the CEL protein as well as other markers of various cellular organelles
3) To characterize the isle functionality by performing glucose-stimulated insulin secretion assay (GSIS)

For aims 2) and 3) wild-type mice and Cel-16R mice were to be used for comparison.

3 Materials

Table 3.1. **Genotyping**

Material	Catalogue number	Supplier
100 bp DNA Ladder	N3231	New England Biolabs
E.Z.D.A DNA tissue DNA kit	D3396-01	Omega Bio-Tek
Ethidium Bromide (0.625 mg/ml)	E406-15ml	VWR
Gel Loading Buffer	G2526-5ML	Sigma Aldrich
Multiplex PCR Kit	206143	Qiagen
SeaKem LE Agarose	50004	Lonza
Tris-Borate-EDTA Buffer x10	A3945	PanReac, AppliChem

Table 3.2. **Pancreas perfusion and dissection**

Material	Catalogue number	Supplier
Syringe without needle, 5 mL	SS-05S	Terumo
HSW FINE-JECT, injection needles, 27G x 1/2 – 0.40 x 12 mm	HK4710004012	Henke Sass, Wolf
Black silk, 3-0, sterile, 100m	14777	Vömel

Table 3.3. **Isolation of pancreatic acini**

Material	Catalogue number	Supplier
100 µm Cell Strainer	431752	Corning
40 µm Cell Strainer	431750	Corning
Accutase Cell Detachment Solution	15323609	Corning
HBSS, calcium, magnesium, no phenol red	14025-092	Gibco
HBSS, no calcium, no magnesium, no phenol red	14175-095	Gibco

Table 3.4. **Isolation of islets of Langerhans**

Material	Catalogue number	Supplier
Histopaque-1077	10771-100ML	Sigma-Aldrich
Histopaque-1119	11191-100ML	Sigma-Aldrich

Table 3.5. **Cell viability assay**

Material	Catalogue number	Supplier
AOPI Staining Solution	CS2-0106-25ml	ViaStain
CellTiter-Glo Luminescent Cell Viability Assay	G7570	Promega
Hydrogen peroxide 30%	1.07298.0500	Supelco
Tunicamycin from Streptomyces sp.	T7765	Sigma-Aldrich

Table 3.6. **DNA quantification**

Material	Catalogue number	Supplier
Absolute alchol prima	600069	Kiiltoclean
Elution Buffer	PDR048	Omega
Hydrochloric Acid	1.09063.1000	Merck

Table 3.7. **Immunofluorescence staining**

Material	Catalogue number	Supplier
Antigen Unmasking Solution, Tris-Based	H-3301	Vector Laboratories
KP Frost Printer Slides - official 90°, but cut edges	PR-001	Klinipath
Normal Goat Serum (10%)	50062Z	ThermoFisher
Paraformaldehyde	P6148	Sigma-Aldrich
ProLong™ Diamond Antifade Mountant with DAPI	P36962	Invitrogen
Round cover glasses (13 mm)	630-2190	VWR
Saponin from *Quillaja saponaria*	S2149	Sigma-Aldrich
Triton X-100	X100-100ML	Sigma-Aldrich
Whatman Puradisc FP 30 mm Cellulose Acetate Syringe Filter, 0.2 µm	10462200	Cytiva's Whatman™

Table 3.8. **Primary antibodies**

Antibody	Catalogue number	Supplier
Anti-Calnexin (Goat polyclonal)	PA5-19169	Invitrogen
Anti-E-cadherin (Rabbit polyclonal)	3195S	Cell signaling
Anti-GM130 (Rabbit monoclonal)	Ab52649	Abcam
Anti-GRP78 BiP (Rabbit polyclonal)	Ab21685	Abcam
Anti-Trypsin (Rabbit monoclonal)	Ab200997	Abcam
As20 (Mouse monoclonal)	Custom made from prof. Olle Hernell	Umeå University

Table 3.9. **Secondary antibodies**

Antibody	Catalog number	Supplier
F(ab')2-Goat anti-Mouse IgG (H+L) Cross-Adsorbed Secondary Antibody, Alexa Fluor 488	A-11017	Invitrogen
Goat anti-Guinea Pig IgG (H+L), Alexa Fluor 546	A-11074	Invitrogen
Goat Anti-Mouse IgG (H+L), Alexa Fluor 594	Ab150116	Abcam
Goat anti-Rabbit IgG (H+L) Highly Cross-Adsorbed Secondary Antibody, Alexa Fluor Plus 594	A32740	Invitrogen

Table 3.10. **Secretion assay**

Material	Catalogue number	Supplier
Amylase Activity Assay Kit	MAK009	Sigma-Aldrich
CCK Octapeptide sulfated, C-terminal ocatapeptide of CCK	ab120209	Abcam
DMEM, high glucose, HEPES, no phenol red	21063029	Gibco
Trypsin inhibitor from soybean	10109886001	Roche

Table 3.11. **Glucose-stimulated insulin secretion assay**

Material	Catalogue number	Supplier
$CaCl_2$	C5670-100G	Sigma Aldrich
D- (+)-Glucose	G8769-100ML	Sigma Aldrich
DPBS	14190-144	Gibco
KCl	60142-100ML-F	Sigma Aldrich
KH_2PO_4	P5655-100G	Sigma Aldrich
$MgSO_4$	M2643-500G	Sigma Aldrich
Mouse insulin ELISA	10-1247-01	Mercodia
Na_2HPO_4	S5136-100G	Sigma Aldrich
NaCl	S5150-1L	Sigma Aldrich
$NaHCO_3$	S5761-500G	Sigma Aldrich
Rapid-Flow Sterile Single Use Vacuum Filter Units	564-0020	Nalgene

Table 3.12. **Common reagents**

Material	Catalogue number	Supplier	Use
Bovine Serum Albumin	82-100-1	Millipore	Acini isolation Glucose-stimulated insulin secretion
Collagenase from *Clostridium histolyticum*	C7657-1G	Sigma-Aldrich	Acini isolation Islet isolation
HEPES (1M)	15630-080	Gibco	Acini isolation Glucose-stimulated insulin secretion
RPMI 1640 Medium, no glutamine	21870076	Gibco	AOPI stain Cellular metabolism assay Islet isolation
Fetal Bovine Serum	10270-106	Gibco	Amylase secretion Islet isolation
Penicillin-Streptomycin	P4458	Sigma-Aldrich	Islet isolation

Table 3.13. **Technical equipment**

Instruments	Manufacture	Use
Gel Doc EZ Imager	Bio Rad	Genotyping
GeneAmp PCR System 9700 thermal cycler	Thermo Fischer Scientific	Genotyping
Leica Confocal SP8	Leica Microsystems	Immunofluorescence
NanoDrop ND-1000	Thermo Fischer Scientific	Genotyping
ThermoMixer C	Eppendorf	Secretion Assay
Varioskan LUX multimode microplate reader	Thermo Fischer Scientific	Luminescence measurement for cellular metabolism assay (ATP)
µDrop Plate	Thermo Fischer Scientific	DNA quantification

Table 3.14. **Analytical software**

Software	Supplier	Use
Asperio ImageScope	Aperio Technologies	H&E-stainings
FIJI software	ImageJ	Immunofluorescence
GraphPad Prism	GraphPad Software, Inc	Cellular metabolism assay and glucose-stimulated insulin secretion
LAS X software	Leica Microsystems	Visualizing images acquired with confocal microscope

4 Methods

4.1 Workflow

In this master thesis, Cel-MODY mice were analyzed and compared with Cel-16R mice expressing the human VNTR with 16 repeats (the most common in the human population) and with the wild-type C57BL/6N mice. The wild-type mice will from now on be referred to as control mice in this thesis. Both Cel-MODY and Cel-16R mice were studied in the heterozygous state. Acini and islets of Langerhans derived from mouse pancreas were purified and studied *in-vitro*. Acini were used for viability assays, immunofluorescence staining, and secretion assay. The secretory capacity of the islets of Langerhans was examined by performing glucose-stimulated insulin secretion assays. An overview of the practical work performed in the thesis is shown in **Figure 4.1**.

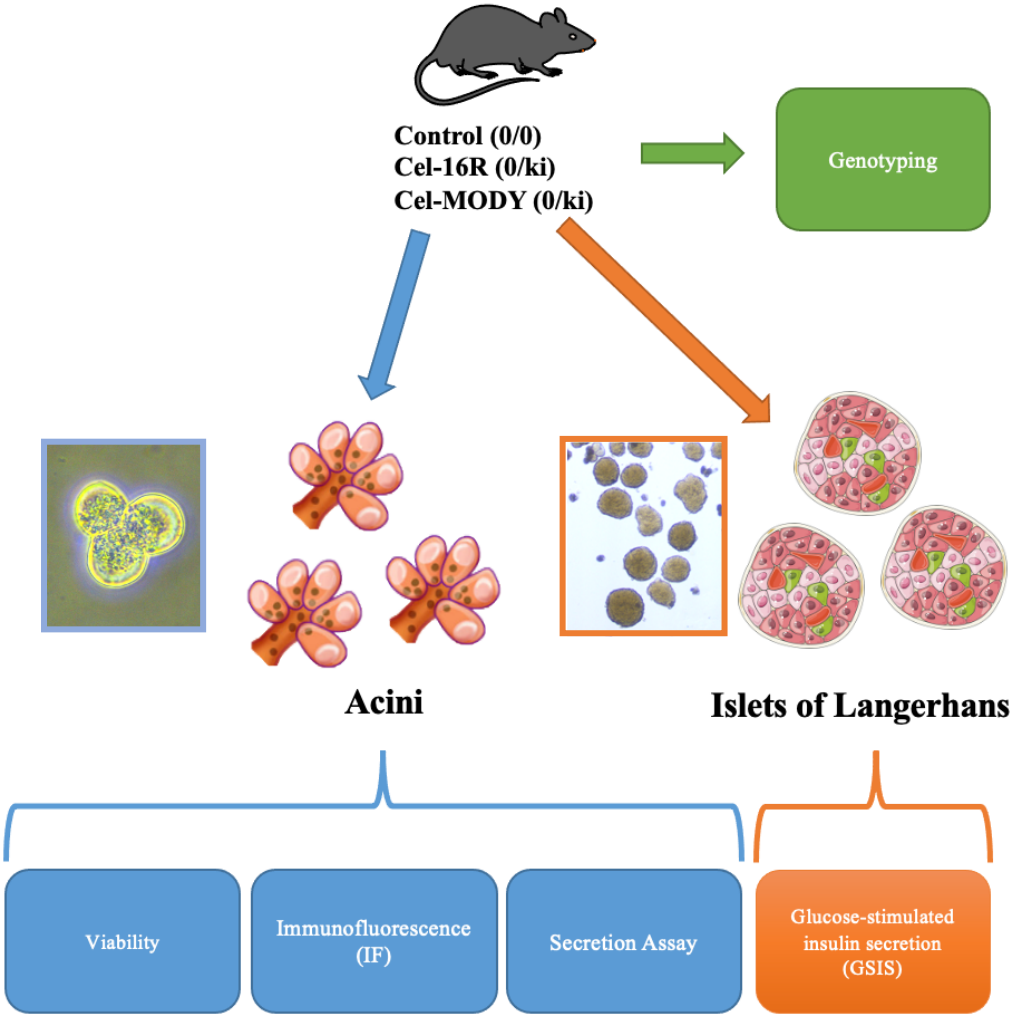

Figure 4.1. **Workflow of the experiments conducted in this thesis**. First, the mouse strains were genotyped to confirm the genetic constitution (green). Mice in the heterozygous state were used to isolate acini (blue) and islets (orange) from the mouse pancreas. The cells were used to perform the different *ex-vivo* experiments listed. Images were acquired with light microscope at 4 X magnification.

4.2 Animals and institutional study approval

This study was approved by Mattilsynet (Norwegian Animal Welfare Agency), FOTS ID 13510, dated 13.12.2017. Both male and female mice of the strain C57BL/6 (between 13 and 15 weeks old) background from GenoWay, Lyon, France were used in this thesis. All mice were bred and kept in cages with 2-6 mice per cage on a 12 h light/dark cycle in the Laboratory Animal Facility, Faculty of Medicine, University of Bergen. The mice were fed with water and standard chow *ad libitum*.

4.3 Genotyping from ear biopsy

Tissue sampling by ear biopsy from two-weeks old mice was used to identify the genotype of newborn pups. Ear biopsy was done by the Laboratory Animal Facility, Faculty of Medicine, University of Bergen, and the tissue was stored at -20 °C. Genotyping was done by the following steps: First, DNA extraction of the ear biopsy was done followed by DNA amplification using polymerase chain reaction (PCR). Finally, the amplification products were analyzed by agarose gel electrophoresis in order to identify the genotype composition for each mouse.

4.3.1 DNA extraction

Genomic DNA was extracted from ear biopsy using E.Z.N.A tissue DNA Kit according to the manufacturer's instructions. The DNA concentration was determined by UV absorbance at OD 260 nm and purity was determined by the ratio at 260/280 using a Nanodrop spectrophotometer.

4.3.2 Polymerase chain reaction (PCR)

Extracted DNA was amplified by using two different polymerase chain reactions (PCR). First, a general PCR was used to differentiate between the wild type (0/0), heterozygous knock-in (0/ki), and homozygous knock-in (ki/ki) of the mouse Cel locus. Then, a specific PCR was used to identify the VNTR region of Cel-WT, Cel-16R, or Cel-MODY. The forward and reverse PCR primer sequences for amplifying genotypes are listed in **Table 4.1**. 30-50 ng of DNA template was amplified in a 25 µl reaction mix containing 5 µM of each primer and 12.5 µl of PCR Master Mix. PCR cycling conditions for general and specific amplification are listed in **Table 4.2** and **Table 4.3**, respectively. The PCR was performed in GeneAmp PCR System 9700 thermal cycler.

Table 4.1. **List of PCR primers used for genotyping for general and specific genotyping reactions.**

Primer		Sequence (5'-3')
General PCR	196271cre-CHU2 (fwd)	GCAAACTTCTTATTTATCCTCAAGCCTTGG
	196272cre-CHU2 (rev)	GTTATCGTCTTAGTGATGTCCAGGTAGTTGC
Specific Cel-16R	0018-TS/PNI (fwd)	CCACCATGAGTCCAATGATTGCACC
	196274oth-CHU2 (rev)	GGTGGCCTCCTGGTCGGTCACT
Specific Cel-MODY	0017-TS/PNI (fwd)	GCCAAAGAGACATGCAGTGAGAAGAGTACC
	198280oth-CHU3 (rev)	CGAATGTCACAGCCCAGAACTTCAGG

Table 4.2. **Steps for PCR program in general amplification of mice genotype.**

PCR Step		Temperature	Time
Pre-heat		95 °C	15 min
35 cycles	Denaturation	94 °C	60 sec
	Annealing	65 °C	90 sec
	Elongation	72 °C	90 sec
Final extension		72 °C	10 min
Hold		4 °C	∞

Table 4.3. **Steps for PCR program in specific amplification of mice genotype.**

PCR Step:		Temperature	Time
Pre-heat		95 °C	15 min
30 cycles	Denaturation	94 °C	30 sec
	Annealing	65 °C	30 sec
	Elongation	72 °C	5 min
Final extension		72 °C	8 min
Hold		4 °C	∞

4.3.3 Agarose gel electrophoresis

The resulting PCR products were separated by electrophoresis in an agarose gel. First, a mix of 12.5 µl of PCR products together and 7.5 µl gel loading buffer were run in a 3 % agarose gel in Tris/Borate/EDTA (TBE) buffer. For band visualization, a drop of ethidium bromide (0.625 mg/mL) was added to the gel and run at 90 V for 1 h. A 100 bp DNA Ladder was used as the DNA standard. The gel bands were visualized under UV-light using a Bio Rad Gel Doc EZ Gel Imager. The expected band sizes of the PCR product are listed in **Table 4.4**.

Table 4.4. **Expected band sizes of the PCR products.**

Allele	Expected PCR product size:
General PCR	
WT	303 bp
Heterozygous	303 bp and 394 bp
Homozygous:	394 bp
Specific PCR	
CHU2-Cel-WT	286 bp
CHU3-Cel-MODY	256 bp
WT	No product

4.4 Hematoxylin and Eosin (H&E)-staining of mouse pancreas

Pancreases from control, Cel-16R and Cel-MODY mice were isolated and fixed in 4 % formaldehyde overnight at RT. The mouse pancreas was embedded in paraffin, sectioning onto SuperFrost Plus Adhesion Slides, and stained with Hematoxylin and Eosin (H&E) by the histology laboratory at the Department of Pathology, Haukeland University Hospital. The slides where scanned and analyzed by using Asperio ImageScope scanner and software.

4.5 Isolation of acini from mice pancreas

For acini isolation mainly females were used. Mice were sacrificed by cervical dislocation following the animal welfare guidelines from Mattilsynet. Then, an incision in the abdominal skin and the subcutaneous layer was made. The pancreas was dissected out followed by incubation with ice-cold collagenase solution (0.2 % Collagenase in HBSS with Mg and Ca). Then, the pancreas was fragmented into smaller pieces, no larger than 2-3 mm^2, using surgical scissors, transferred into a 50 mL conical tube, and then incubated in a water bath at 37 °C for 13-15 min for digestion. During the incubation, the samples were shaken every 2-3 min until the suspension turned homogenous with no obvious undigested fragments. Once the digestion was completed, the reaction was stopped by adding ice-cold washing solution (0.1 % BSA and 10 mM HEPES in HBSS). The disaggregated tissue was washed 2 times with this solution by centrifugating at 1500 rpm for 2 min before filtering through a 100 μm mesh to remove larger tissue debris. The tube was centrifuged once more, and the resulting acini were resuspended in the buffer of interest.

4.6 Isolation and purification of islet of Langerhans

The summarized protocol is depicted in **Figure 4.2**. For islet purification only males were used (13-15 weeks of age). Prior to cervical dislocation, body weight and blood glucose values were taken from each mouse. The mice were opened by an incision in the abdominal skin and subcutaneous layer by surgical scissors (**Figure 4.3 A**). The pancreas was then perfused with freshly prepared collagenase solution (0.1 % Collagenase in PRMI with 5 % FBS) into the ampulla of Vater (**Figure 4.3 B**). The goal is to force the collagenase to enter the pancreatic duct and flush the entire organ (**Figure 4.3 C and D**). The bile duct and the lower part of the duodenum were sealed before perfusion to block the pathway to the liver, gall bladder, and intestine.

If the pancreas was not fully inflated (partially successful perfusion), the collagenase solution was injected directly into the pancreas (**Figure 4.3 E**). Successful perfusion is obtained when all regions of the pancreas are fully inflated (**Figure 4.3 F**). The inflated pancreas was carefully dissected out and fragmented into smaller pieces and placed in a 50 mL conical tube.

Collagenase digestion was carried out in a water bath temperature at 37°C for 13-18 minutes and the tube was shaken by hand during the incubation until the suspension turned homogenous. Once digested, the enzymatic digestion was terminated by adding ice-cold washing solution (RPMI and 5 % FBS). The disaggregated tissue was washed 2 times with the washing solution by centrifugation at 1500 rpm for 2 min before filtering through a ~1 mm mesh to remove larger tissue debris. The cells were washed one more time before a density gradient was prepared to separate islets of Langerhans from pancreatic acini. The cells were dissolved in 5 mL heavy Histopaque (1.119 g/mL), before carefully adding an additional 15-mL layer of light Histopaque (1.077 g/mL). 5 mL of the washing solution constituted the final layer (**Figure 4.4 A**). The gradient was centrifuged at 2400 rpm for 20 min with low acceleration and no brake to achieve best separation of structures. Separation is obtained because intact islets of Langerhans will be found in the interface between the washing solution and the light Histopaque while the reaming exocrine material forms a pellet at the bottom of the tube (**Figure 4.4 B and C**).

Purified islets were harvested into a new tube and washed with the washing solution 3 times. The islets were resuspended in 10 mL of washing solution and transferred into a Petri dish. A second purification of islets from the exocrine tissue was done to further increase islets purity.

The islets were handpicked after identifying them using a light microscope. Islets were transferred to a new Petri dish containing fresh sterile RPMI supplemented with 10 % FBS and 1 % P/S for overnight incubation in a humidified atmosphere with 5 % CO_2 at 37 °C.

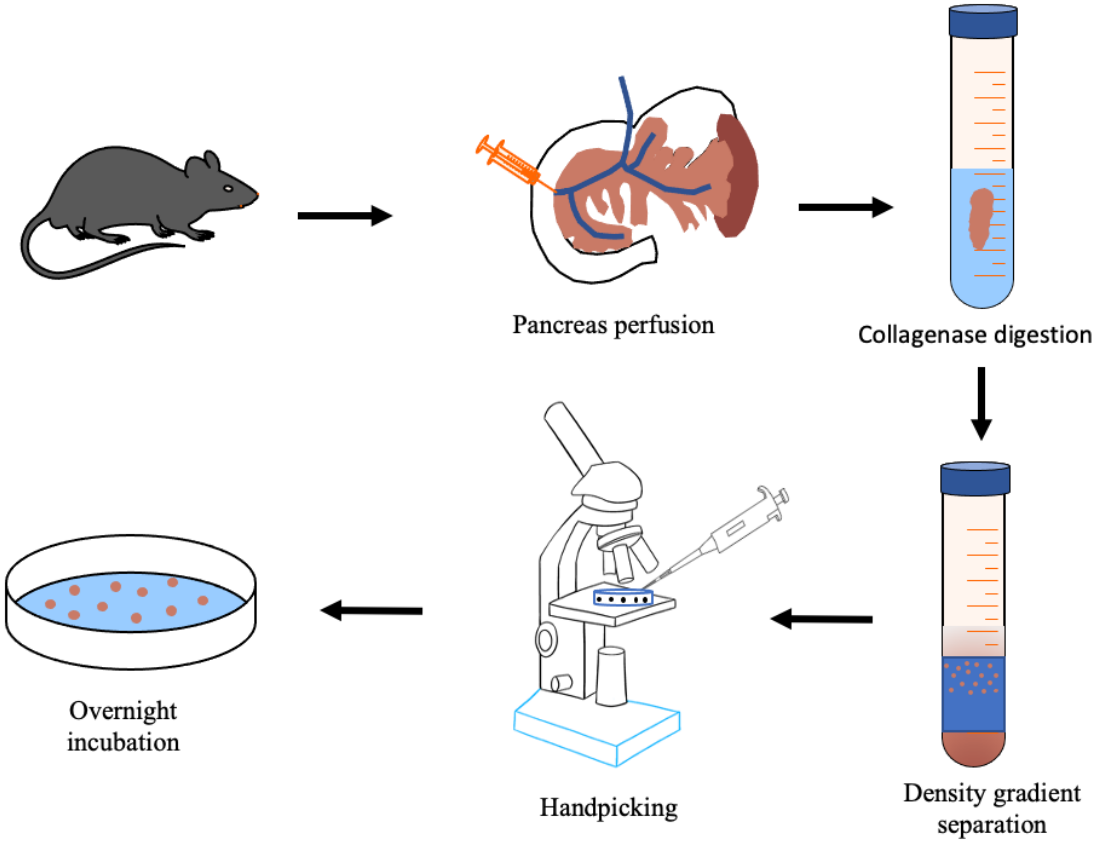

Figure 4.2. **An experimental outline for isolation of islets of Langerhans from mice**. The mouse was first sacrificed and opened, before doing a pancreas perfusion with a collagenase solution. The inflated pancreas was dissected out and digested in a water bath. A density gradient was made to separate the islets of Langerhans from remaining the exocrine material. The islets were handpicked by using a light microscope to enrich the islets of Langerhans before an overnight incubation for recovering the purification.

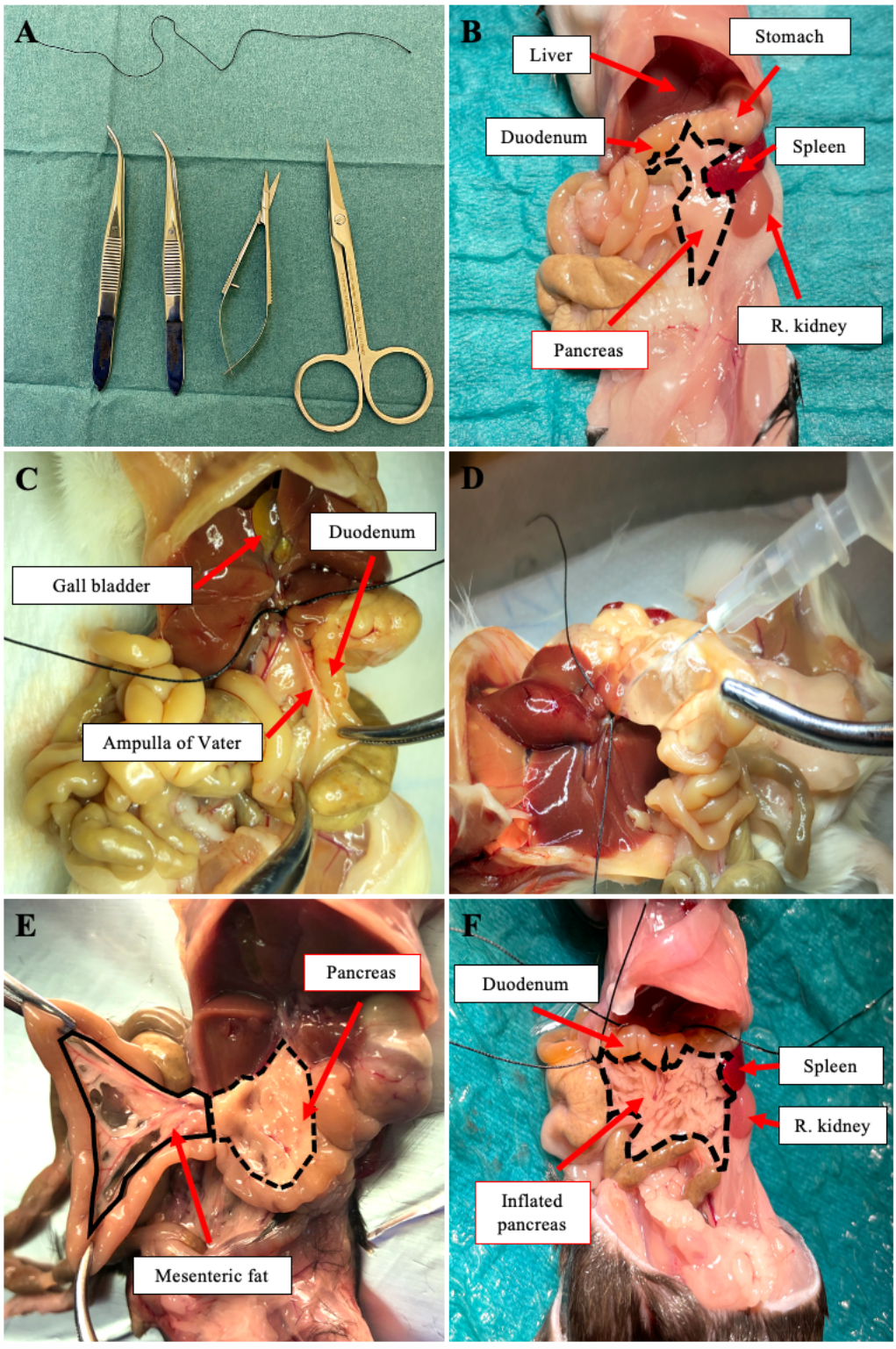

Figure 4.3. **Perfusion of the mice pancreas. A)** Surgical tools used for isolation of islets of Langerhans: curved forceps, micro- and normal surgical scissors **B)** Localization of the pancreas and adjacent organs after the incision of the abdominal skin and subcutaneous layer. The dotted line shows the boundary of the pancreas. **C)** Location of Ampulla of Vater, connecting the duodenum and the pancreas. **D)** Injecting the collagenase to the pancreas through Ampulla of Vater. The bile duct is sealed with a thread (close to the gall bladder), while the lower part of the duodenum is sealed with a forceps, so the collagenase does not go to the liver or gall bladder though the

systemic ducts or the intestine through the duodenum. **E)** The mesenteric fat and the pancreas located in the intestinal system. The dotted line shows the boundary of the pancreas, while the solid line shows the mesenteric fat. **F)** Fully inflated pancreas after perfusion with collagenase and adjacent organs. The dotted line shows the boundary of the pancreas.

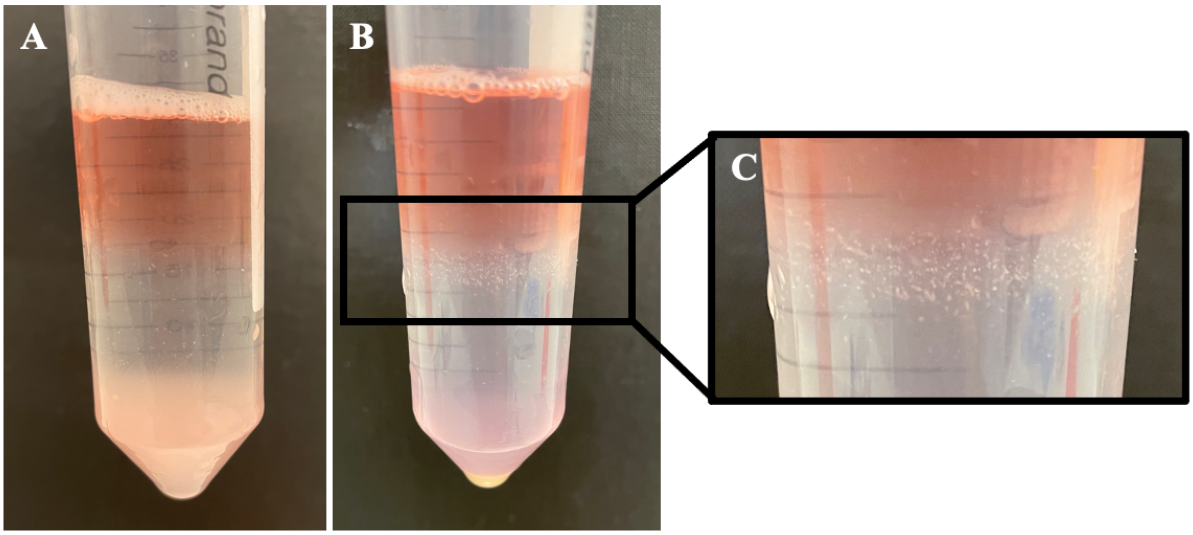

Figure 4.4. **Separation of islets of Langerhans using a Histopaque density gradient**. The procedure is used to isolate intact islets of Langerhans from the remaining exocrine material. **A)** Density gradient before centrifugation. The cells were dissolved in the heavy Histopaque (1.119 g/ml)- Light Histopaque (1.077 g/ml) was carefully added and RPMI constituted as the final layer. **B)** Density gradient after centrifugation at 2400 rpm for 20 min (low acceleration and brake). Exocrine cells form a pellet at the bottom of the tube, while islets of Langerhans migrate to the interface between the RPMI and Histopaque (1.077 g/mL). **C)** Close up of the interface containing the islets. Islets of Langerhans appears as white dots that can be seen with the naked eye.

4.7 Functional characterization of isolated acini

Freshly isolated pancreatic acini from MODY, 16R, and control mice (all in heterozygous state) were used in different *ex-vivo* experiments to characterize their function. Cellular viability was examined by dual nucleic acid binding dyes Acridine Orange and Propidium Iodide (AOPI) and cellular metabolism assay as well as the secretion capacity after CCK stimulation. Moreover, acini were also fixed and stained by immunocytochemistry.

4.7.1 Cell viability assay by using Acridine Orange and Propidium Iodide

Isolated acini were detected AOPI staining and investigated under a fluorescent microscope to visualize living and dead cells. The permeable AO stains all nucleated cells (both alive and dead cells) to generate green fluorescence, while impermeable PI stains only dead nucleated cells with compromised membranes (red fluorescence). Due to the Förster resonance energy

transfer, all live nucleated cells appear as green while all the dead nucleated cells appear as red in the fluorescent microscope (Mitchell, 2012). The isolated acini cells were transferred into a Petri dish containing fresh RPMI supplemented with 10 % FBS and 1 % P/S. A 1:1 dilution of the AOPI-stain was added to the acini cells at different time points. The cells were incubated in sterile medium in a humidified atmosphere with 5 % CO_2 at 37 °C, when the cells there not visualized with AOPI.

4.7.2 Dissociation of acini into single cells and cell viability assay

Isolated acini cells were treated with Accutase to dissociate them into single acinar cells. 1 mL of Accutase was incubated with the acini at 37 °C for 30 min, with gentle pipette mixing every 5 mins. To stop the reaction RPMI supplemented with 5 % FBS and 1 % PS was added, and the cellular solution was filtered through a 40 μm cell strainer to collect single cells. The cells were then washed 3 times with RPMI media and centrifugated at 1500 rpm for 2 min.

Acinar cells (100 μl) from each mouse strain were transferred into a 96-well plate and treated with 1 mM H_2O_2, 5 μg/ml tunicamycin, or 20 μg/ml tunicamycin to induce oxidative stress and ER stress, respectively. The cells were incubated at 37 °C for 30 min. Control wells were prepared containing medium without cells to obtain a value for background luminescence. Cellular viability was measured in triplicates by using CellTiter-Glo Luminescent Cell Viability kit. In brief, 100 μl of CellTiter-Glo Reagent containing a lyophilized enzyme/substrate mixture was added to each well containing the cell suspension; the cells were then mixed for 2 min on an orbital shaker to induce cell lysis, before incubating the plate at room temperature for 10 min to stabilize the luminescent signal. The luminescence was recorded with an integration time of 1 sec per well by a Varioskan LUX multimode microplate reader.

The biochemical background of the assay relies on the luciferase reaction which requires ATP and Mg^{2+} as co-factors to convert luciferin to oxyluciferin; this causes the release of luminescence as measurable energy (**Figure 4.5**). Because the recorded luminescence signal is directly proportional to the amount of ATP present in the cells, it can be used as a measurement for metabolic activity in the cells.

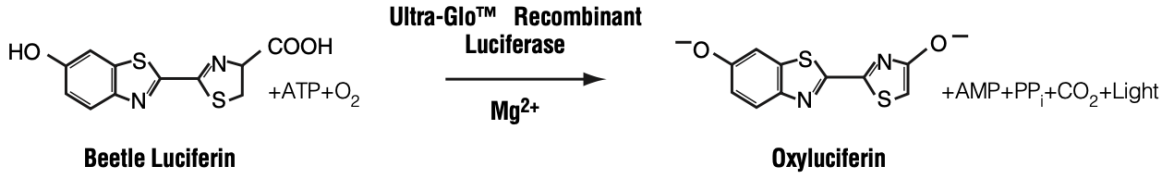

Figure 4.5. **The luciferase reaction**. Luciferase converts luciferin in presence of ATP, Mg^{2+}, and molecular oxygen to oxyluciferin and luminescence as byproduct.

4.7.3 Immunofluorescence on freshly isolated acini

In the acinar cells, CEL as well as other digestive enzymes display a very characteristic intracellular pattern, with the majority of the protein being stored in the zymogen granules at the apical site facing the lumen of the acini. In order to be able to compare the subcellular distribution of the CEL protein in the different mouse strains to examine whether the MODY8 acinar cells show any alteration in the secretory pathway, immunofluorescence with a CEL-specific antibody was performed. The stainings were done in suspension and the different solutions containing primary or secondary antibodies were exchanged by centrifugating at 1500 rpm during 5 min at 4°C. In order to maintain the intracellular morphology of the cells intact and stop all biological processes, the cells were immediately fixed (3 % PFA in PBS) for 30 min as quickly as possible and right after the isolation of the acini. Then, the acini were permeabilized (0.1 % Triton-x100 in PBS) for 10 min to allow the antibodies to be able to penetrate the cell membrane and access to intracellular antigens. After that, the acini were blocked (10 % goat serum) for 1 h to avoid non-specific binding of antibodies to macromolecules within the cells. The acini were incubated with primary antibodies (**Table 4.5**) diluted in washing solution (2 % BSA and 0.2 % Saponin in PBS) and incubated overnight at 4 °C with a gentle shake. Next day, the cells were washed for 2 h with the washing solution, the solution was changed twice during the washing time. The fluorophore-conjugated secondary antibody was added at a 1:500 dilution in washing solution for 1 h, before washing the cells for 2 h in the washing solution.

If a double IF procedure was performed, the second antibody was added for overnight incubation, following the same procedure. The antibodies against CEL protein and E-cadherin were used in double staining, while the others were applied individually. Before mounting, the acini were washed with MQ-water twice. The cells were mounted with Pro-Long Gold mounting medium, stored at RT for 1 day and then at 4 °C until confocal microscopy visualization.

One exception in this protocol was staining with trypsin for which the acini were blocked (10 % goat serum) for 15 minutes. Cells were then subjected to antigen retrieval in Tris-based antigen unmasking solution and boiled at 85 °C for 5 minutes. The acini were blocked again (10 % goat serum) for 1 h. The rest of the procedure was performed as described previously.

Table 4.5. **Primary antibodies used for immunofluorescence in acinar cells**. The antibody dilution, the specificity and the corresponding fluorophore-conjugated secondary antibody used are listed.

Primary Antibody	Dilution	Secondary Antibody	Marker
CEL (As20)	1:20	Anti-Mouse A488	CEL protein
BiP	1:50	Anti-Rabbit A594	Hsp78 chaperon protein, marker of ER stress
Calnexin	1:100	Anti-Goat A488	ER
E-cadherin	1:200	Anti-Rabbit A594	Plasma membrane
GM130	1:300	Anti-Rabbit A594	Cis-Golgi
Trypsin	1:100	Anti-Rabbit A594	Zymogen granules

4.7.4 Confocal imaging

Stained cells were imaged with a Leica TCS SP8 STED 3x confocal microscope (Leica Microsystems) with lightning deconvolution mode. A continuous wave laser of 405 nm and WLL 70 % was used to image the stained acini. Oil was used as immersion medium on a HCX PL APO CS 100x objective (NA 1.4). The images were acquired with the LasX software and modified with Fiji software. Highest resolution was used with a pinhole size ranging from 0.2-0.5 and zoom on 2.

4.7.5 Amylase secretion assay of acini

Acinar cells produce and secrete digestive enzymes. Amylase secretion assay was performed to investigate the secretory capacity of freshly isolated acini. Cholecystokinin octapeptide (CCK-8) was used as a stimulating agent in different concentrations to make a secretion curve. The concentrations used were 0, 10^{-12}, 10^{-11}, 10^{-10}, 10^{-9}, 10^{-8}, 10^{-7}, and 10^{-6} M for a full curve. The secretagogue was diluted in phenol red-free DMEM supplemented with 5 % FBS and 0.1 mg/ml trypsin inhibitor. Media with the different CCK-8 concentrations were added to the acini and incubated at 37 °C under continuous shaking at 600 rpm for 30 min on a ThermoMixer C.

After stimulation, the media were collected by centrifugating at 1500 rpm for 5 min and frozen at -20°C until quantification of amylase activity.

To evaluate amylase secreted by primary acini, the enzymatic activity was measured using an amylase activity assay kit according to the manufacturer's instructions. Each sample (20 µl) was measured with a 1:50 dilution and adjusted to a final volume of 50 µl with Amylase Assay Buffer. The amylase enzymes are glycoside hydrolases and cleaves glucan linkages in polysaccharides. The assay use ethylidene-pNP-G7, an α-amylase substrate. The amount of substrate is proportional to the product, p-nitrophenol in nmole/well (405 nm). Amylase concentration was determined by UV absorbance at 405 nm by using a Varioskan LUX multimode microplate reader.

4.8 Functional characterization of freshly isolated islets of Langerhans

To functionally assess the insulin production and secretory function, freshly isolated islets of Langerhans from Cel-MODY, Cel-16R and control mice (all in heterozygous state) were stimulated *ex-vivo* to secrete insulin by incubating them with different amount of glucose.

4.8.1 Glucose-stimulated Insulin Secretion (GSIS)

After the islet isolation procedure (described above) the islets were incubated overnight in high glucose medium (RPMI). Next day healthy-looking islets (n=25) of approximately the same size (70-100 microns) were carefully handpicked and aliquoted in each tube. The islets were first rinsed with pre-warmed washing solution (0.5 % BSA in PBS) 3 times during 10 min. Then, the islets were starved with no glucose in freshly made Krebs buffer (KRB) (129 mM NaCl, 5 mM $NaHCO_3$, 4.8 mM KCl, 2.5 mM $CaCl_2$, 1.2 mM $MgSO_4$, 1 mM Na_2HPO_4, 1.2 mM KH_2PO_4, 10 mM HEPES, 0.1% BSA) for 30 min in a water bath at a temperature of 37°C. The media was collected and replaced with KRB buffer containing low glucose (1.67 mM glucose) in the same conditions and eventually the media was collected. Next, the islets were incubated with KRB buffer containing high glucose (20 mM glucose) and media was also collected. Finally, an incubation in KRB buffer containing KCl and high glucose (30 mM KCl and 20 mM glucose) for 20 min, was carried out and the media was collected. All collected media samples were centrifuged at max speed for 15 min to remove unwanted cells and the supernatant was transferred into a new tube. The measurements were performed in triplicate assays, containing 25 islets each.

The release of insulin during the GSIS was measured with an enzyme linked immunosorbent assay (ELISA) kit specifically designed for mouse insulin and following the manufacturer's protocol. All samples needed to be diluted 1:10 and were measured in duplicates.

4.8.2 DNA concentration measurements from islets after GSIS

Right after the GSIS, the islets were centrifuged at max speed for 15 min to remove the supernatant. The islets pellet was frozen at -20°C, then 100 µl of acid-ethanol (1.5 % HCl with 70 % EtHO) was added for lysis and the solution was left to evaporate overnight. 10 µl of elution buffer was added to the tube in order to measure the DNA concentration using Varioskan LUX multimode microplate reader with a µDrop Plate. The values were used to normalize the insulin concentration measured by ELISA.

4.9 Statistical analysis

All statistical analysis were performed using GraphPad Prism 9. Two-way ANOVA was used for multiple comparison of the results from cellular metabolism, amylase secretion, and GSIS. $P < 0.05$ was considered statistically significant.

5 Results

5.1 Genotyping of transgenic Cel-MODY and Cel-16R mice

DNA was extracted from ear marks and used as a PCR template to verify the genotypes of transgenic Cel-MODY and Cel-16R mice. Two different PCR reaction were used: a general PCR to detect the transgenic VNTR sequence of the mouse *Cel* locus to distinguish between control (0/0), heterozygous (0/ki), and homozygous (ki/ki) animals, and a specific PCR to confirm the exogenous VNTR of Cel-MODY or Cel-16R transgenic mice. Agarose gel electrophoresis was done for visualizing the PCR product of the general and specific reaction. Results of the genotyping of the transgenic Cel-MODY and Cel-16R mice are shown in **Figure 5.1**.

Verification of general PCR product in agarose gel is shown in **Figure 5.1 A and B**. Expected band for wild-type allele are at 303 bp. Two lanes from both Cel-MODY and Cel-16R are observed with one band at ~300 bp indicating the samples originate from a control mouse. The heterozygous allele is expected to show bands at 303 bp and 394 bp, one lane from Cel-MODY and two lanes from Cel-16R shows two bands at ~300 bp and ~400 bp in the gel indicating the presence of heterozygous allele. One lane from Cel-MODY shows a band at ~400 bp, demonstrating homozygosity from the Cel-MODY allele (394 bp).

Verification of specific PCR product in agarose gel is shown in **Figure 5.1 C and D**. Expected band for exogen VNTR for Cel-MODY are at 256 bp and Cel-16R at 286 bp. One band appeared in two lanes from Cel-MODY and Cel-16R at ~300 bp, indicating the presence of exogen VNTR. In the remaining lanes, no bands were present, showing that the mice are controls.

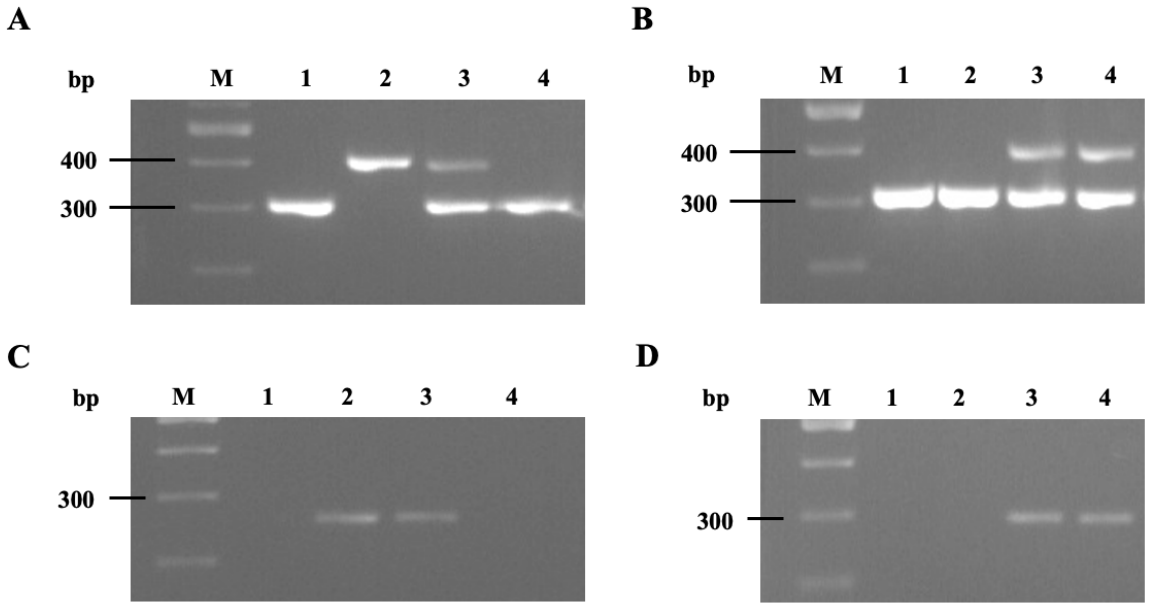

Figure 5.1. **Genotyping of Cel-MODY and Cel-16R mice**. DNA from transgenic mice was amplified with PCR and analyzed in ethidium bromide-stained 3 % agarose gel. The marker in bp is marked with "M" in the figure. A) Results of the general PCR amplification for Cel-MODY. In lane 1 and 4, one band was observed at 300 bp, indicating control (0/0) mice. One band at ~400 bp is found in lane 2, indicating the homozygous (ki/ki) allele. Lane 3 shows two bands at ~400 bp and 300 bp, indicating heterozygous (0/ki) mice. B) Results of the general PCR amplification for Cel-16R. Lines 1 and 2 show control mice with one band observed at ~300 bp, while lines 3 and 4 show heterozygous (0/ki) mice, with two detected bands at ~400 and 300 bp. C) Results of the specific PCR amplification for Cel- MODY. No bands are detected in lines 1 and 4, confirming the control animals in A. One band at ~300 bp is found in lanes 2 and 3, confirming Cel-MODY. D) Results of the specific PCR amplification for Cel-16R. In lanes 1 and 2, no band is detected, confirming the WT in B. One band at ~300 pb is found in lanes 3 and 4, indicating Cel-16R.

5.2 Pancreas histology in the Cel-MODY mice

Pancreases from Cel-MODY, Cel-16R, and control animals, along with the spleen and a portion of the duodenum were collected. The organs were paraffin-embedded and tissue sections were stained for H&E. Hematoxylin stains the nucleic acids with a deep blue-purple color, while eosin stains cytoplasm pink.

Examples of the pancreas histology of control and Cel-MODY animals are shown in **Figure 5.2** and **Figure 5.3** respectively. The histology of the pancreas from Cel-16R looks similar to the control mouse and is not shown. Control and Cel-16R mice showed normal pancreatic morphology of both the exocrine and endocrine tissues. The size and the distribution of islets of Langerhans varied between the different lobes of the pancreas. Only some pancreatic

sections from Cel-MODY mice had a pathological phenotype. Fat infiltration and replacement in the exocrine tissue were evident, although the phenotype varied between the lobes. The islets found in the section look normal.

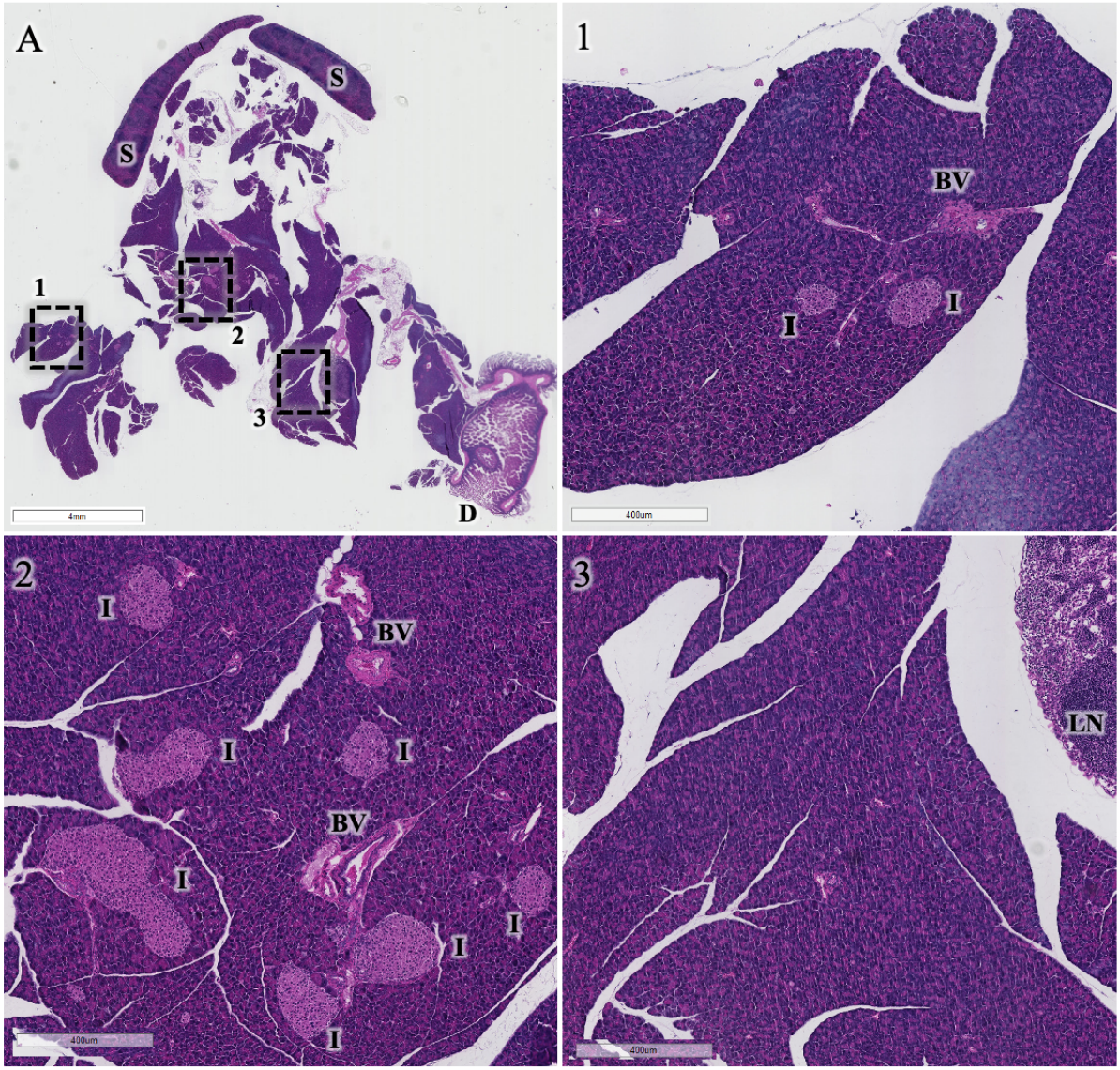

Figure 5.2. **H&E-staining images of pancreas isolated from a 3-month old control mouse. A)** Whole section showing the pancreas, spleen (S), and a part of the duodenum (D). Squares with numbers 1, 2, and 3 indicate areas shown with higher magnifications in the other images. Scale bar= 4 mm **1, 2, and 3)** Number and size of islets vary considerably between lobes. Scale bar=400 µm. Abbreviations: S, spleen; D, duodenum; BV, blood vessel; I, islet of Langerhans, and LN, lymph node.

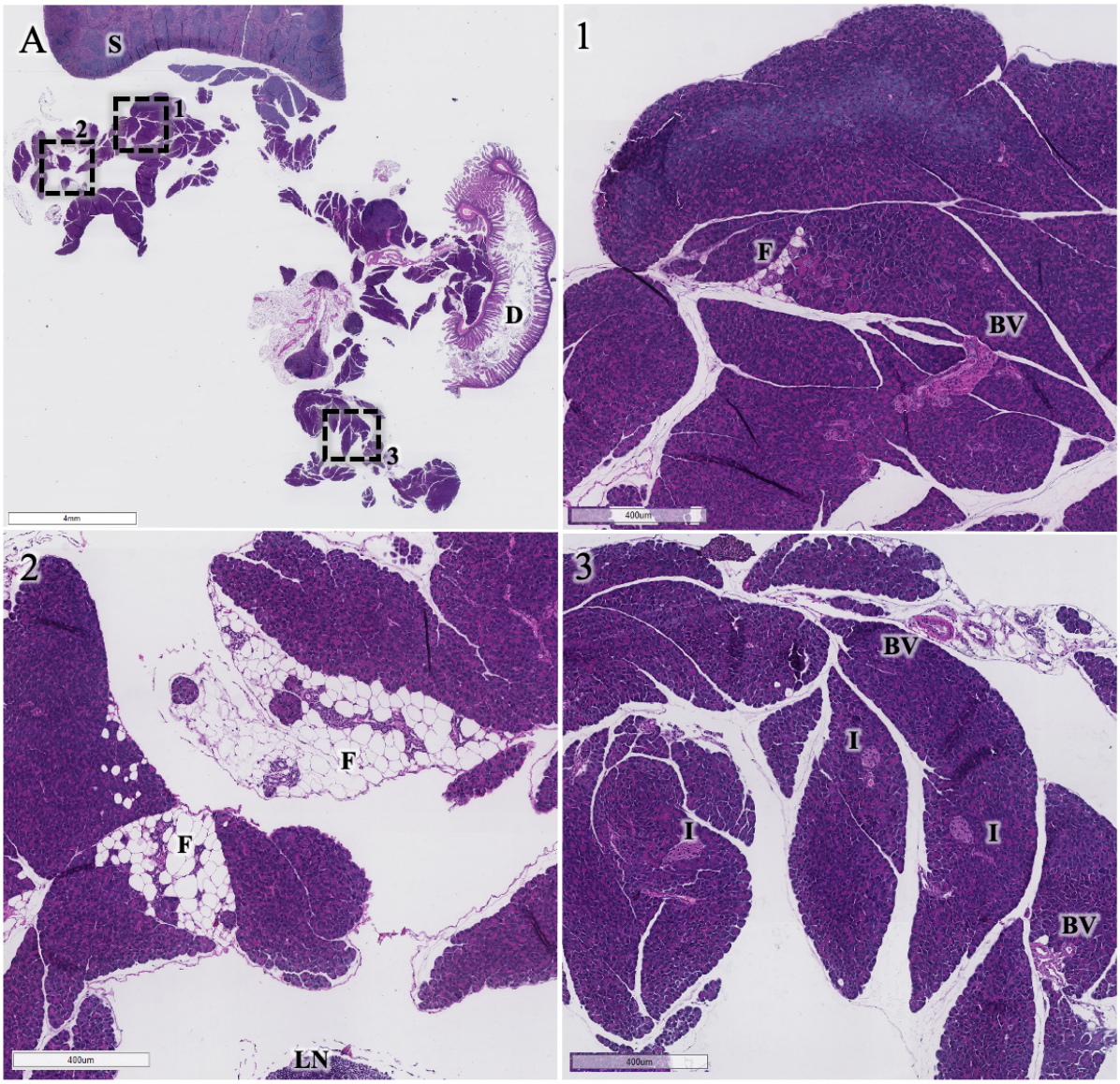

Figure 5.3. **H&E-staining images of pancreas isolated from 3-month old Cel-MODY mice. A)** Whole section showing the pancreas, spleen (S), and a part of the duodenum (D). Squares with numbers 1, 2, and 3 indicate areas shown with higher magnification. Scale bar= 4 mm. **1 and 2)** Fat replacement in the exocrine tissue vary considerably between lobes. Scale bar= 400 µm **3)** Islets with normal morphology. Scale bar= 400 µm. Abbreviations: D, duodenum; S, spleen; F, fat; BV, blood vessel; LN, lymph node; I, islet of Langerhans.

5.3 Body weight and glucose measurements in mice

Both males and female mice from the Cel-MODY, Cel-16R, and control strains were used in the study. Each mouse was weighed before the endpoint which was between 13 weeks to 15 weeks. Blood glucose levels were also measured for the males whose islets were to be used in the glucose-stimulated insulin secretion assay. Mice body weight and blood glucose levels are shown in **Figure 5.4**. There were no significant differences in weight for males, females, or blood glucose levels within each group.

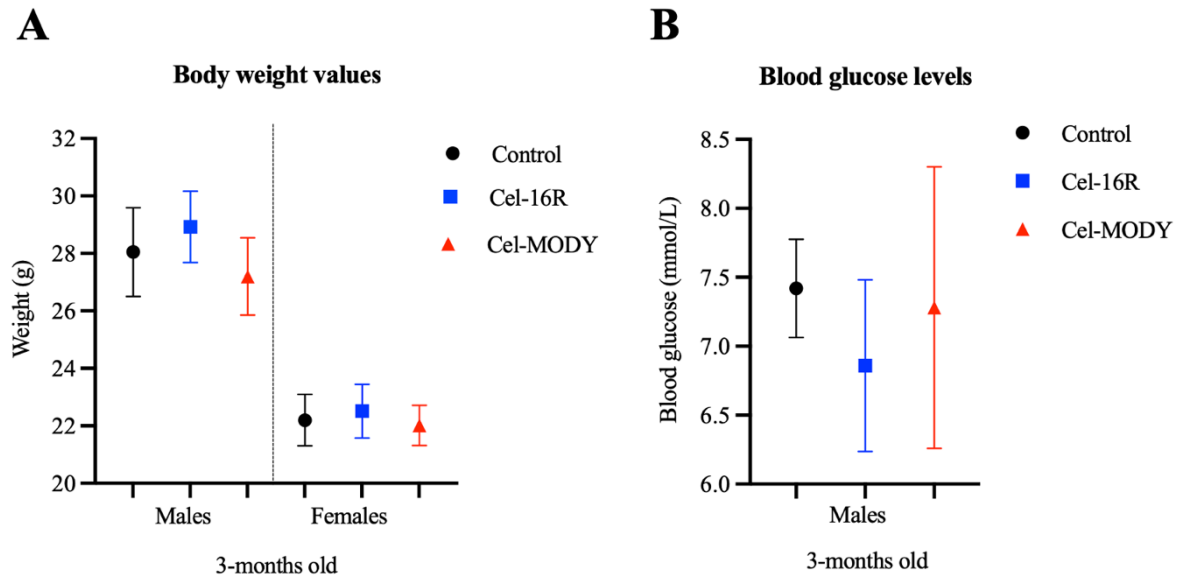

Figure 5.4. **Weight and blood glucose levels of the three different mice strain used at 3-month old. A**) Body weight (g) is presented as the mean for males and females (N=8). **B**) Blood glucose levels (mmol/L) is presented as the mean for males (N=5). Error bar represents the standard deviation.

5.4 Assessment of acini function

5.4.1 Morphological analysis of cell viability

Double staining with Acridine Orange and Propidium Iodide (AOPI) was applied to investigate the viability of isolated acini from mouse pancreas. These combined stains consist of two nucleic acid binding dyes: AO which forms green fluorescence on live nucleated cells and the PI that produces red fluorescence in all dead nucleated cells. The isolated acini were observed and cultured over a time period of up to 7 days. Fluorescent microscopy was used to visualize the cells.

In **Figure 5.5** fluorescent images of the isolated acini from the three mouse strains, Cel-MODY, Cel-16R, and controls are shown. The cells were examined both immediately after isolation and 3 h post isolation with few dead cells observed, mostly at the periphery of the acini. After 2 days there were still no marked differences. Thereafter, on day 3 the cells started to change their morphology, where acini seemed to cluster against each other and form spherical clusters of cells of various sizes. Surprisingly, these clusters of cells were still alive on day 7 with a more circular structure. Overall, no striking differences were seen in the cell viability between the acini isolated from the Cel-MODY, Cel-16R, and the control mice. However, the acini pellet purified from Cel-MODY was smaller than that from the Cel-16R and control mice, and

consequently, the number of cells left on Petri dish was also reduced for every day. On day 7 of the experiment, there were barely any cells left.

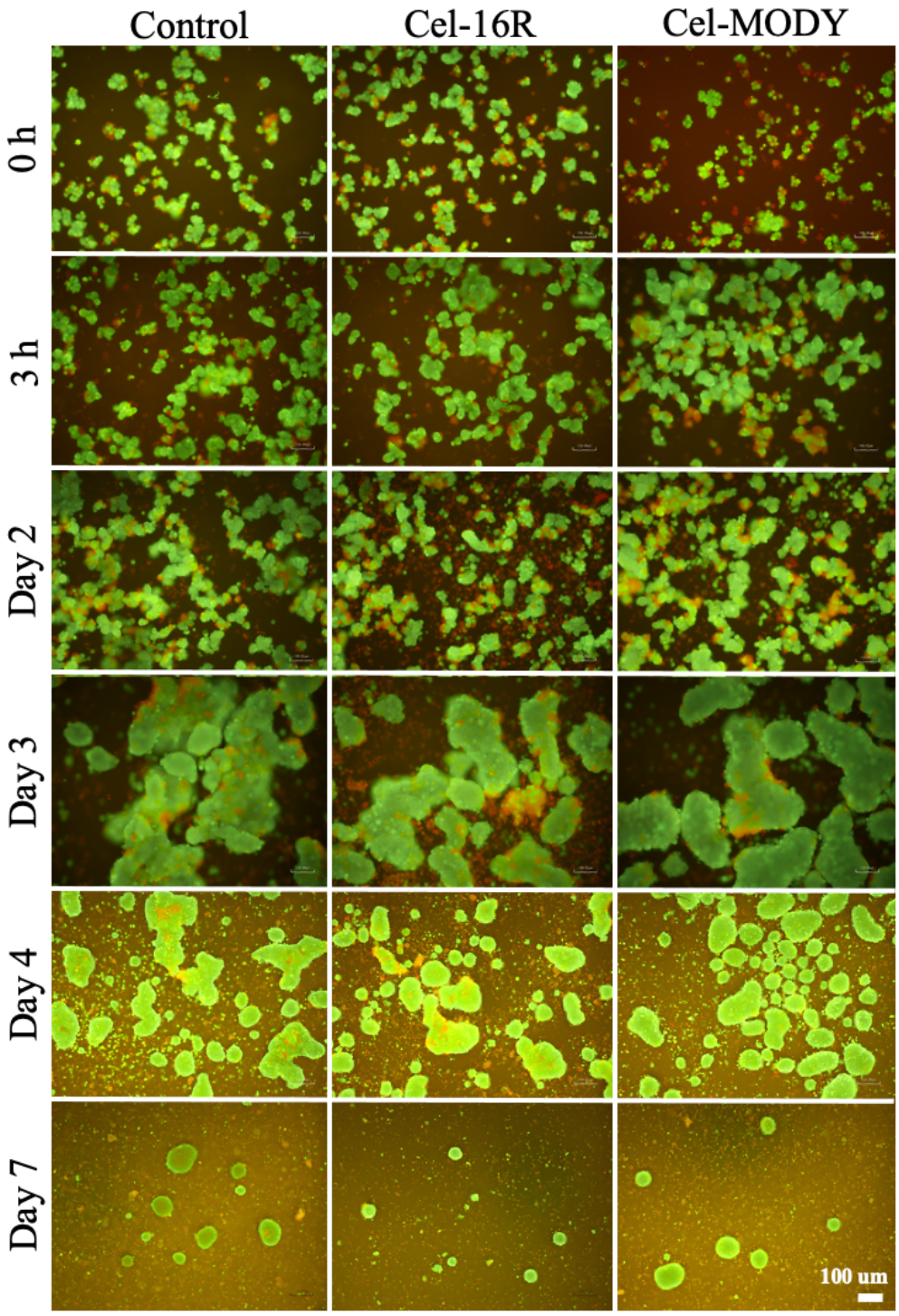

Figure 5.5. **Cell viability examined with Acridine Orange and Propidium Iodide (AOPI) double staining in isolated acini.** Cellular viability was observed right after and 3 h after isolation as well as at days 2, 3, 4 and 7. Green fluorescence indicates live nucleated cells and red fluorescence indicates dead nucleated cells. Images were acquired with light microscope at 4 X magnification. Scale bar 100 µm.

5.4.2 Cellular metabolism assay

The cellular metabolism of the isolated acinar cells from the three different mice strains was compared. For this, the CellTiter-Glo luminescent assay was employed. Since the reaction requires ATP, the luminescence signal is proportional to the amount of ATP present in the cells, as a global indicator for cellular metabolism. The isolated acini were treated with Accutase to dissociate them into single acinar cells. The acinar cells were treated with H_2O_2 and tunicamycin to induce oxidative stress and ER stress, respectively.

First, AOPI was added to the cells to evaluate the cell viability after the dissociation with Accutase, an enzyme mixture with proteolytic and collagenolytic enzyme activity that allows the detachment of cells. Fluorescent images of AOPI-stained acini after further cell dissociation are shown in **Figure 5.6.** Some of the acini were dissociated into single acinar cells, while some remained as smaller clusters composed of 2-3 cells. There were no large differences between the mice strains in neither structure nor the cell viability although more dead cells (red nuclei) could be appreciated after the treatment with Accutase in Cel-MODY mice.

Quantification of the metabolic activity is shown in **Figure 5.7**. Each experiment was done in three technical triplicates. As expected, untreated cells gave the highest intracellular ATP level. Treating the cells with both H_2O_2 or tunicamycin showed a decrease in metabolic activity, which is expected with the well-known effects of H_2O_2 or tunicamycin in causing oxidative and ER stress, respectively. Treating the cells with 20 μg/ml tunicamycin results in the lowest amount of ATP indicating that the cells were undergoing major cell death regardless of their phenotype. Moreover, the metabolic activity of acinar cells isolated from Cel-16R mouse seemed to be less affected at small doses of both reagents, which was contrary to what was seen in acinar cells from Cel-MODY mice. Acinar cells from Cel-MODY mice were seen to significantly contain the lowest levels of ATP ($P<0.0001$) even in cells that were not treated. In addition, H_2O_2 and tunicamycin triggered cell death in these cells as deduced from the low levels of ATP to an extent that was higher than in the control and Cel-16R cells. These results could be indicating that Cel-MODY mice were already fragile and struggle to maintain a healthy ER.

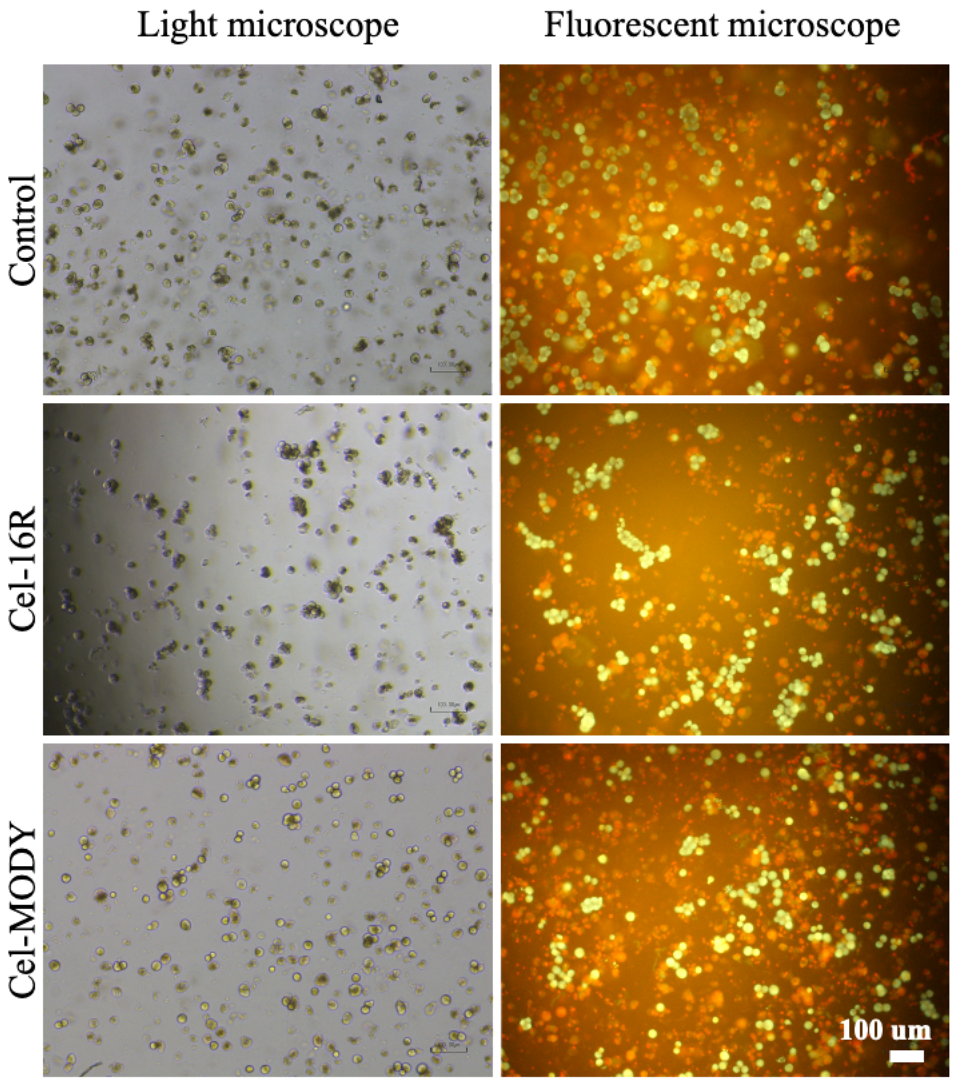

Figure 5.6. **Morphology of acinar cells after dissociation by using Accutase followed by AOPI-staining**. The acini were dissociated into single acinar cells before performing the cellular metabolism assay. Acridine Orange and Propidium Iodide staining was used to evaluate cell viability. Green fluorescence indicates live nucleated cells and red fluorescence indicates dead nucleated cells. Images were acquired with a light microscope (left) and fluorescent microscope (right) at 100 X magnification. Scale bar 100 µm.

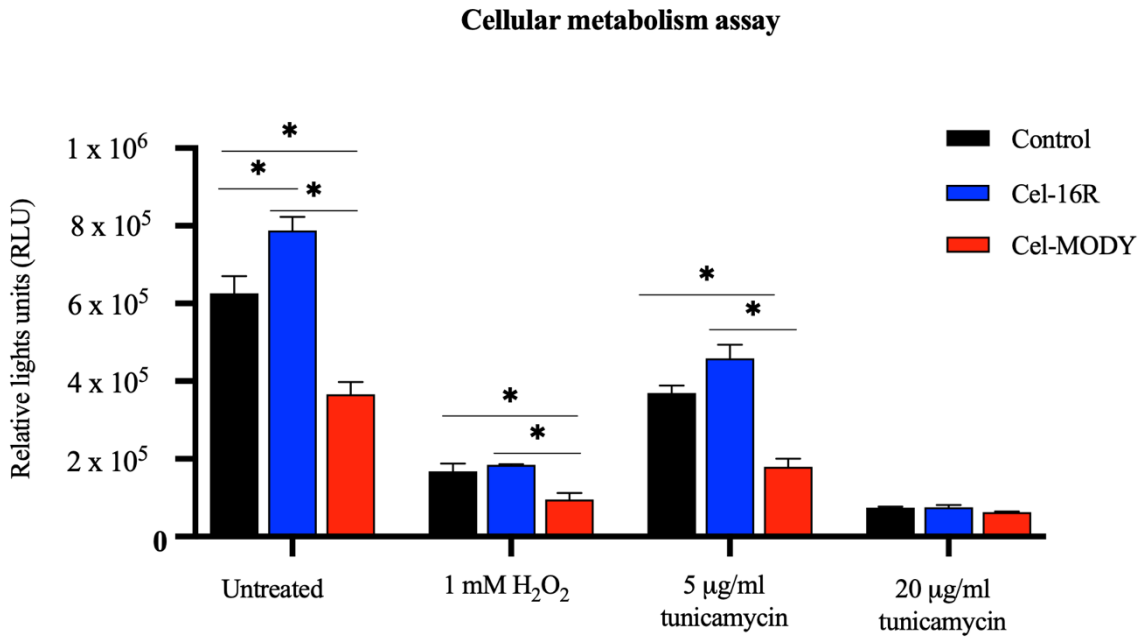

Figure 5.7. **Cellular metabolism assay after treatment with H_2O_2 and tunicamycin in isolated acinar cells**. The bar graphs illustrate the amount of ATP present in acinar cells isolated from control, Cel-16R, and Cel-MODY mice. The experiment was performed in triplicates. Treatment with 1 mM H_2O_2, 5 µg/ml tunicamycin, and 20 µg/ml tunicamycin were used to induce oxidative and ER stress, respectively. The relative light units (RLU) signal is proportional to the amount of ATP in cells. *P< 0.0001. Error bar represents the standard deviation.

5.4.3 Protein distribution in isolated acini

Acini isolated from mice strains were stained with different markers to investigate the protein distribution within the cells. After isolation, the acini were fixed and double-stained with CEL together with E-cadherin; the latter is a marker for the plasma membrane included in order to see the delimitation of individual acinar cells. The nuclei were visualized by using DAPI (blue).

Confocal images of double-staining of CEL together with E-cadherin are shown in **Figure 5.8**. Each staining was performed in three independent experiments with similar results. The green signal shows the intracellular distribution of CEL whereas the red fluorescence is labeling plasma membrane E-cadherin. In the acini from control and Cel-16R mice, the staining pattern was characterized, mostly, by an apical distribution of the protein which is stored within the zymogen granules. These granules, however, displayed a slightly different distribution in the MODY mice acini. Instead of being confined to the apical part of the acinar cells and facing the lumen of the acini, the CEL-containing granules were also present in the basolateral sides of the cells in a slightly tubular shape.

The acini were also stained for calnexin, BiP, GM130, and trypsin alone to examine whether any distribution differences within the ER, Golgi network, or the zymogen granules could be detected. Confocal images of single staining of various cellular organelles are presented in **Figure 5.9**. Each staining was performed in three independent experiments with similar results. Acini were stained with antibody against GM130, a marker for cis-Golgi (red fluorescence). Acini were also stained for calnexin, which is an integral membrane protein of the ER (green fluorescence). As a marker of ER stress was used BiP, an HSP78 chaperon protein (red fluorescence). Trypsin was used as a marker for zymogen granules due to the storage of trypsin in the granules in the acinar cells (red fluorescence). There was no marked difference between the staining of the different mice strains.

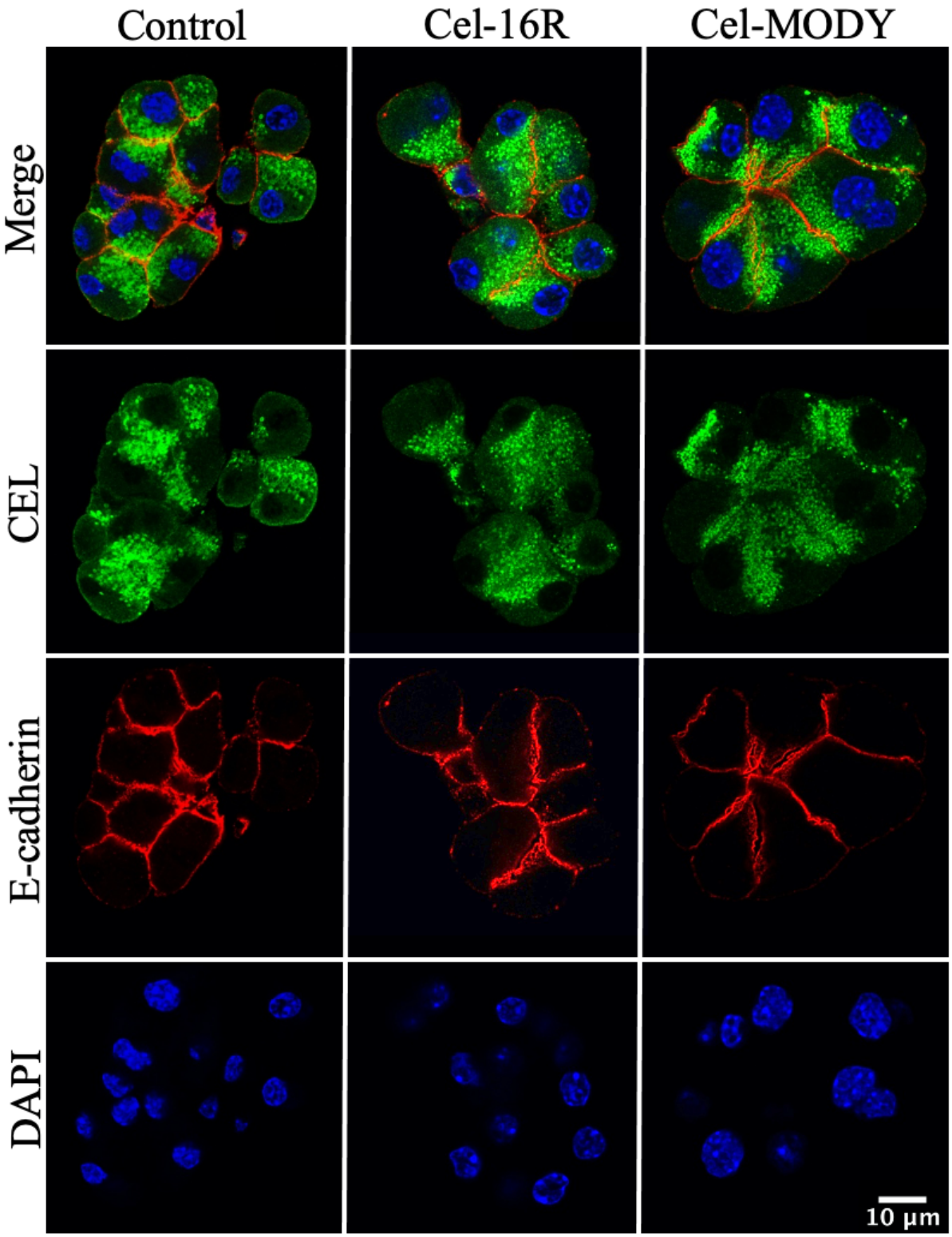

Figure 5.8. **Subcellular localization of CEL protein and E-cadherin in freshly isolated acini.** Isolated acini from Cel-MODY, Cel-16R, and control mice were fixed and stained for CEL protein and E-cadherin. Green fluorescence indicates CEL protein staining, red fluorescence indicates E-Cadherin staining and blue fluorescence indicates DAPI staining for cell nuclei. Images were acquired by a confocal microscope at 100X magnification. Scale bar 10 µm. Data are representative of three independent experiments with similar results.

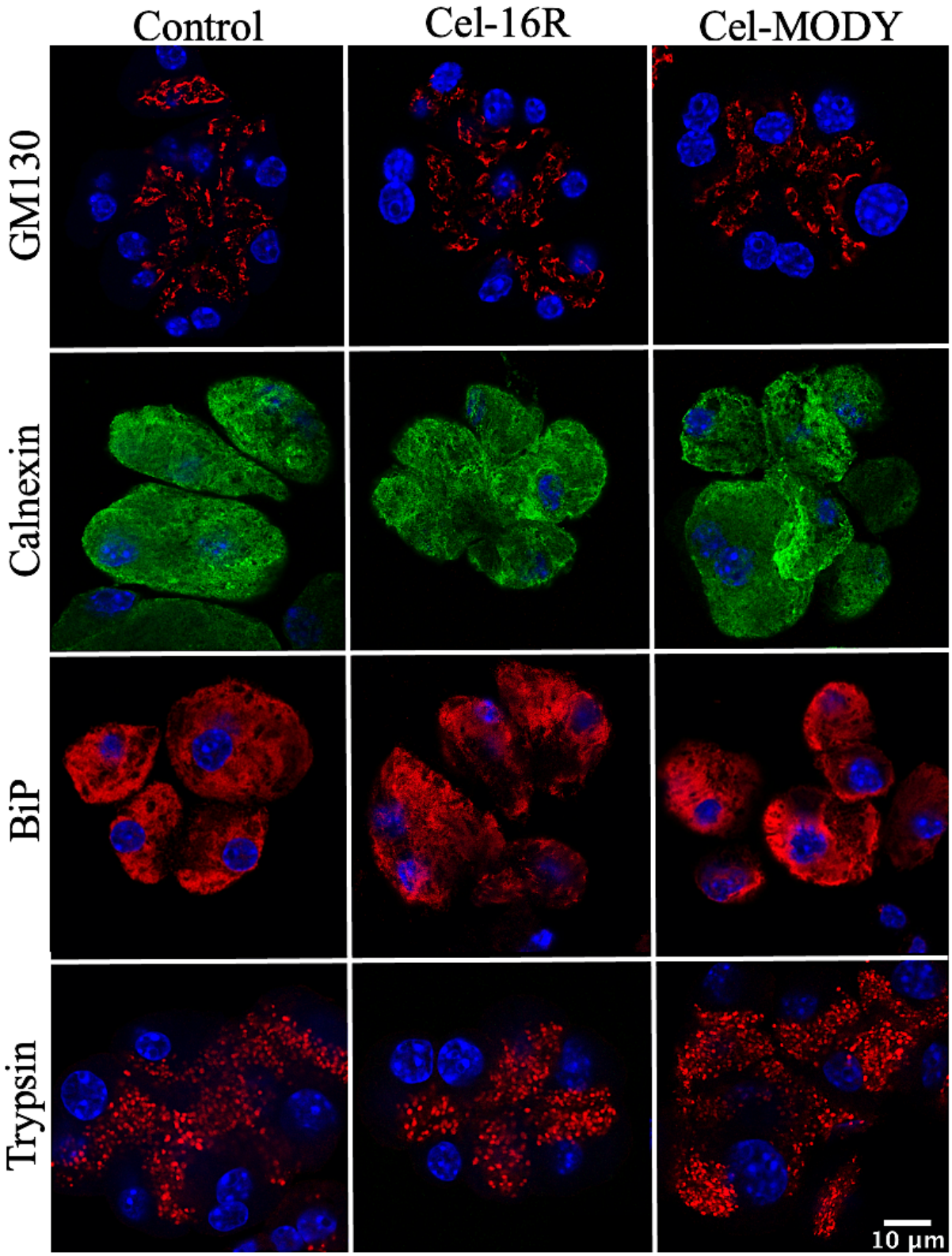

Figure 5.9. **Intracellular localization in acini of various markers of cellular organelles.** Isolated acini from Cel-MODY, Cel-16R, and control mice were fixed and stained for GM130, calnexin, BiP, and trypsin. The DAPI staining (blue) was used to visualize nuclear morphology. Images were acquired by a confocal microscope at 100X magnification. Scale bar 10 µm. Data are representative of three independent experiments with similar results.

5.4.4 Secretory capacity of pancreatic acini

The amylase secretion assay was performed to investigate the secretion of digestive enzymes of acini as this assay can serves as a global measure for the secretion capacity of acini. Isolated acini were stimulated with different concentrations of CCK-8 to obtain a full curve response and the released amylase was measured.

The dose-response curve for amylase secretion is shown in **Figure 5.10**. Three independent experiments were performed on both control and Cel-16R acini, whereas two independent experiments were performed for Cel-MODY acini. CCK-8 level induced amylase secretion in all mice strains, and maximal-stimulating CCK-8 concentration was 10^{-11} M. The acini were observed not to respond to high concentrations of CCK-8 (10^{-6}, 10^{-7}, and 10^{-8} M). The secretion on acini isolated from Cel-MODY was lower at all CCK concentrations, and significant difference were seen untreated cells ($P<0.0001$) and at 10^{-7} M ($P<0.01$) compared to control mice. However, there was not observed a statistically significant differences at the concentration (10^{-11} M) that resulted in peak activity.

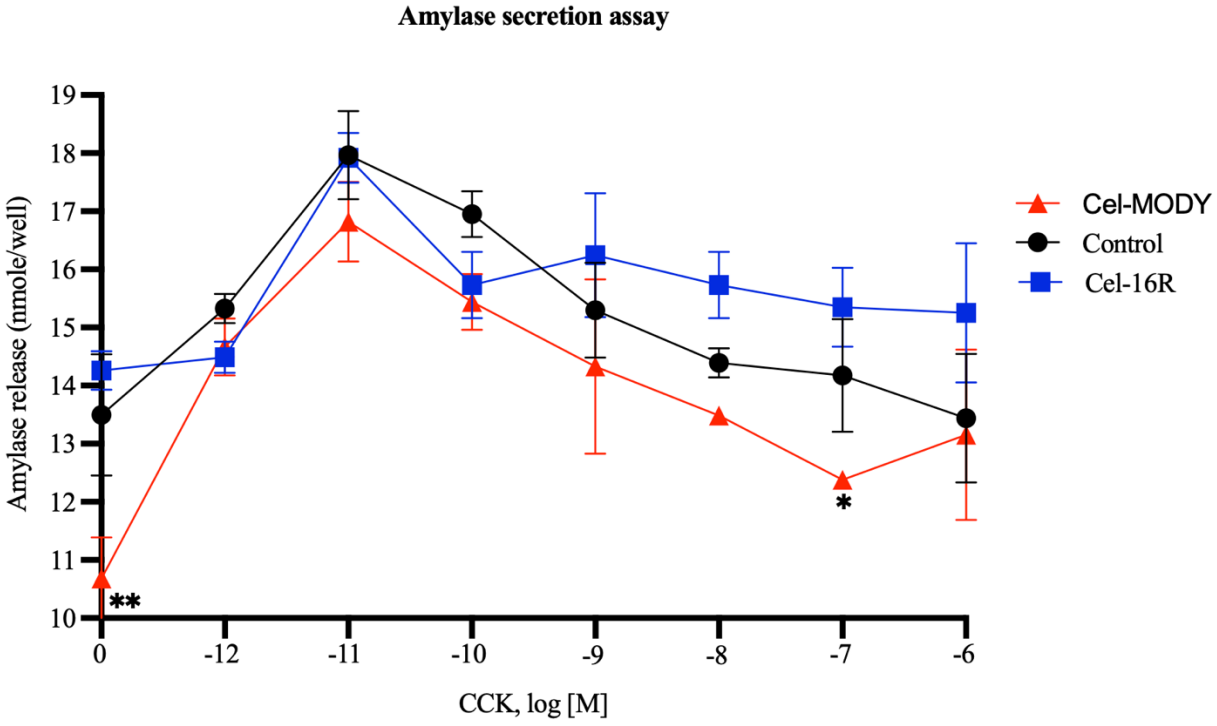

Figure 5.10. **CCK-8-induced amylase secretion from acini isolated from control, Cel-16R, and Cel-MODY mice**. Results are presented as the mean of amylase secreted (nmole/well) by different stimulating concentrations of CCK. Error bar represents the standard deviation of three independent experiments for control and Cel-16R, while Cel-MODY represents two independent experiments. *P< 0.01 and **P<0.0001 compared to control mice.

5.5 Functional assessment of islets of Langerhans

5.5.1 Islet yield and purity

Pancreatic islets of Langerhans were isolated from Cel-MODY, Cel-16R, and control mice. The pancreas was digested with collagenase, washed by centrifugation, filtered to remove tissue debris, followed by separating of the intact islets by a density gradient. The islets were collected and washed, before transferring into a Petri dish to enrich the islets by handpicking using a light microscope.

The morphology of isolated islets of Langerhans after the isolation (day 1) and after overnight incubation (day 2) is shown in **Figure 5.11**. The typical morphology of islets is a spheroid shape with various sizes and a distinct brownish color in the light microscope. Right after isolation (day 1), the islets appear with slightly irregular borders. The islets were held in culturing media for overnight incubation to allow the living islets to recover from the isolation procedure. After overnight incubation (day 2), islets recovered to appear with a smoother and more regular spherical shape with well-defined borders.

The yield was found to be 100-300 islets/mouse in control and Cel-16R mice compared to ~50-50 islets/mouse in Cel-MODY mice. There was not observed a significant difference in islets size between the three groups. The islets size was measured to be 50-250 µm in diameter in all experiments.

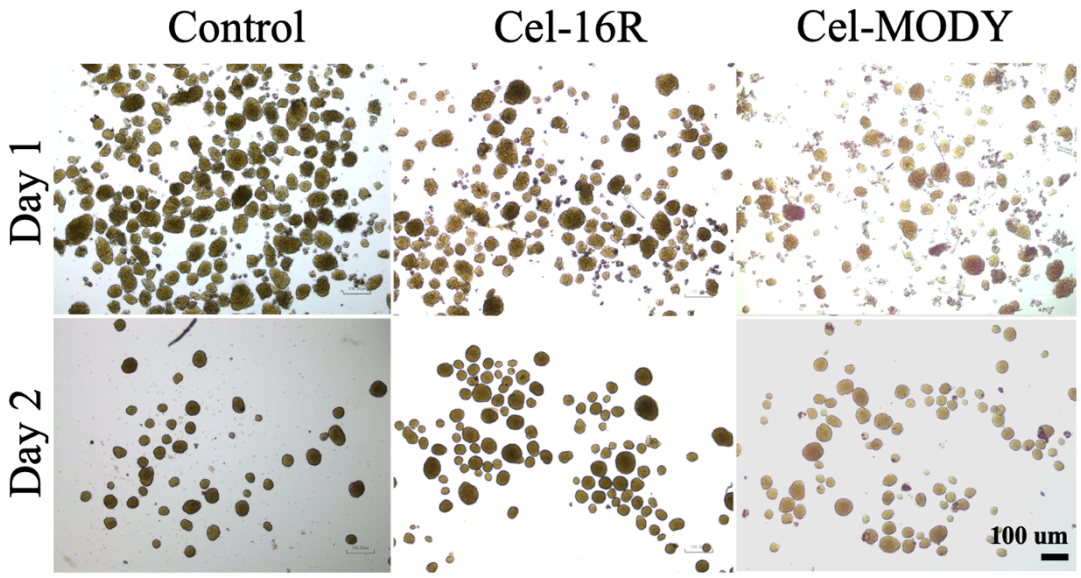

Figure 5.11. **Morphology of islets of Langerhans following isolation.** Isolated islets were purified from Cel-MODY, Cel-16R, and control mice. Day 1 islets are shown right after isolation and day 2 islets represent the result after overnight incubation. Images were acquired with light microscope at 4X magnification. Scale bar 100 µm.

5.5.2 Insulin secretion by glucose stimulation

Different amount of glucose in addition to KCl was added to the isolated pancreatic islets for investigating insulin secretion. The 1-day incubated islets in RPMI with 10 % FBS and 1 % PS were used to assess the potency of islet function by Glucose Stimulated Insulin Secretion (GSIS). Three solutions were used to incubate islets; 1. Low glucose, 2. High glucose, 3. High glucose and KCl. The supernatant was collected after every step and the insulin secretion was determined by ELISA.

The results for the secretion assay are shown in **Figure 5.12**. Each experiment was done in three technical triplicates. Insulin secretions correspond to the extracellular concentration of glucose among all mice strains. No supply of glucose results in no insulin secretion and increased glucose levels resulted in increased insulin levels, as expected. Islets of Langerhans isolated from Cel-16R mice appeared to have the generally highest insulin secretion compared to Cel-MODY and control mice. However, there were no significant differences between the mice strains.

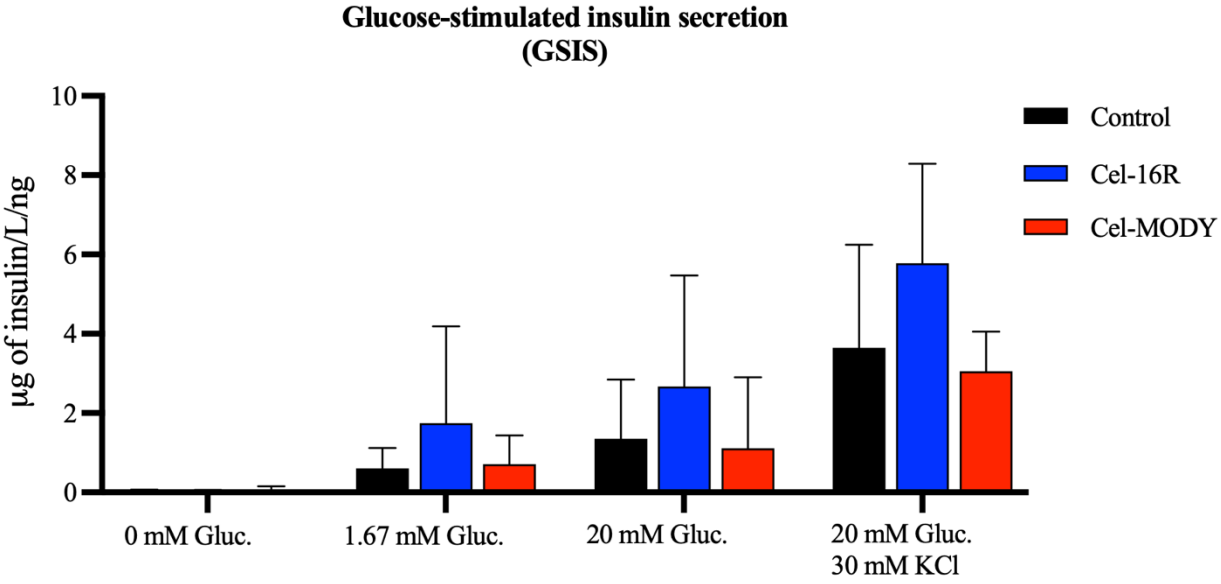

Figure 5.12. **Glucose-stimulated insulin secretion (GSIS) assay of isolated islets from control, Cel-16R, and Cel-MODY mice**. The experiment was done in triplicate, each measuring insulin secretion from 25 isolated islets of the mouse strain. After overnight incubation, isolated islets were incubated in KRB buffer with no glucose (0 mM, 15 min). Islets were then stimulated with basal low glucose (1.67 mM, 30 min), then high glucose (20 mM, 30 min), and high glucose with KCl (20 mM and 30 mM, respectively, 15 min). The supernatant was collected, and insulin content was measured by ELISA. Results are presented as µg of insulin/L/ng of DNA. Error bar represents the standard deviation.

6 Discussion

6.1 Mouse models for the CEL-MODY syndrome

CEL-MODY is an inherited autosomal dominant disease affecting both the exocrine and endocrine pancreas. Single-base pair deletion in the *CEL* gene leads to a syndrome classified as a monogenic form of diabetes because the causative mutation leads to diabetes. This uncommon disease is characterized by the onset of diabetes before the age of 25 years, irreversible pancreatic exocrine dysfunction which is manifested by low fecal elastase levels and steatorrhea, and accompanied by the development of multiple pancreatic cysts, lipomatosis (fat infiltration), and atrophy (Ræder et al., 2007; Ræder et al., 2006; Tjora et al., 2013).

Several cellular studies investigating the disease mechanism of CEL-MODY have been done since our group reported mutation in the VNTR repeat of the *CEL* gene in 2006 (Ræder et al., 2006). Our group has used HEK293 cell line and shown that the mutant CEL-MODY protein has reduced stability and a higher tendency to form both intra- and extracellular aggregates (Johansson et al., 2011). Protein aggregation may lead to proteotoxicity, increased ER stress, activation of the unfolded protein response, and mediated cell death by apoptosis (Gravdal et al., 2021; Johansson et al., 2011; Torsvik et al., 2014; Xiao et al., 2016). CEL-MODY is therefore believed to be a protein misfolding disease that might involve a negative gain-of-function effect caused by mutations in the *CEL* gene (Johansson et al., 2011).

Two animal models have previously been investigated in our group for the purpose of studying the CEL-MODY syndrome at organ level. Vesterhus et al. studied a knock-out mouse model with deletion of the *CEL* gene, and in their study, they reported no pathogenic phenotype of the pancreas pathology, which demonstrated that the disease was more complex than just removing the CEL function (Vesterhus et al., 2010). In a second attempt, Ræder et al. established a mouse line carrying a mutation in the human *CEL* gene and crossed with elastase-Cre mouse line, resulting in over-expression of the disease-associated mutation in *CEL* gene (Ræder et al., 2013). Also, this mouse model resulted in no pathological phenotype. Suggested explanations were a high copy number of the transgene which can lead to silencing of gene expression (Garrick et al., 1998). The phenotype could also be caused by differences between species in the regulation of *CEL* expression (Ræder et al., 2013).

Recently, our group has developed a knock-in mouse model where the mouse endogenous VNTR region of the CEL gene was replaced with the human CEL VNTR, containing the same one base pair deletion as seen in one of the Norwegian families where the disease was discovered. This mouse model shows features of diseases in the exocrine pancreas similar to those seen in patients. Fat replacement within the exocrine tissue and loss of acinar cell tissue (atrophy) was seen as early as in 3-month old heterozygous mice. Contradictive to what has been seen in humans, the Cel-MODY knock-in mice were not hyperglycemic. For the 3-month old Cel-MODY mice used in this thesis, normoglycemia was observed (values 5.8-8.7 mmol/L). These values are within the normal range of glucose levels for C57BL/6 (Rodriguez-Diaz et al., 2018). Neither at 6- nor at 12-months of age did these mice were shown to be hyperglycemic (Gravdal et al, unpublished). The disease is progressive, and at 3 months of age, the pathological features we observed were less prominent than in mice of age 6 months or older (Gravdal et al, unpublished).

6.2 Assessment of acini function

6.2.1 Isolation, culture, and viability of freshly isolated acini

Several methods have been described for culturing acinar cells (Logsdon & Williams, 1986; Williams, 2010; Williams et al., 1978). Acini can maintain the integrity up to 24-48 h in two-dimensional (2D) cultures but lose their secretory capability and polarity after 6 h (Gout et al., 2013; Williams, 2010). This makes it challenging to culture acinar cells for long-lasting studies (Bläuer et al., 2014). Surprisingly, our acini were still alive at day 7 post isolation, but abnormal cell morphology could be observed on day 3 after isolation. Culturing primary acini within a three-dimensional (3D) culture can extend the acini cell viability up to 7-10 days *in-vitro* (Gout et al., 2013; Williams, 2010).

Although it was beyond the scope of this thesis, it would be interesting to see whether the acinar cell's ability to produce and secrete digestive enzymes is maintained after long-term culturing. The numbers of dead acinar cells were expected to increase every day, but the AOPI-staining did not show many dead cells at the end of the experiment. This could be explained by that acini contains extensive amounts of digestive enzymes; these enzymes might be released and digest acini with fragile membranes, causing rapid apoptosis in these cells. However, no obvious differences were seen in the morphology between acini isolated from Cel-MODY mice compared to the control mice. In our experience, the pelleted material after isolation of acini

from Cel-MODY mice was smaller than the pellets arising from the two control strains. This could be due to the loss of acinar tissue mass and subsequent replacement by adipocytes in Cel-MODY mice.

6.2.2 Metabolic activity of isolated acini

The cellular metabolic activity between the mice strains was observed to be significantly reduced in primary acinar cells isolated from Cel-MODY mice compared to the two control mice. This could indicate that pancreas from Cel-MODY mice were already fragile and struggled to maintain healthy. In order to verify the negative effect of H_2O_2 or tunicamycin on the viability of pancreatic acinar cells, we measured the metabolic activity by quantifying intracellular ATP levels in acinar cells. H_2O_2 and tunicamycin cause oxidative and ER stress, respectively, and induce apoptosis in cells. Treatment with these substances resulted in substantially lower metabolic activity in all mice strains which confirms that the cells do undergo major cell death, regardless of their phenotype.

A challenge for this assay was to normalize the number of cells used in each mouse strain. Different methods were tried such as stain the cells with trypan blue and count by using a cell counter, count by using flow cytometry, and quantify the DNA concentration. The challenge was that some of the acinar cells were still in clusters and not fully dissociated to single cells.

6.2.3 Intracellular distribution of CEL and other markers of the secretory pathway

Like other digestive enzymes produced and secreted by the acinar cells, the CEL protein is synthesized and correctly folded in the rough ER. Here it undergoes post-translational modifications such as N- and O-glycosylation, phosphorylation, and disulfide-bond formation. CEL is thereafter transported to the Golgi apparatus for complete O-glycosylation and once it is fully processed, it is densely packed into zymogen granules that undergo trafficking to the apical part of the cells and, upon stimulation, it will be secreted by exocytosis into the lumen of the acini (Johansson et al., 2018; Logsdon & Ji, 2013).

In the staining performed on freshly isolated acini, the CEL protein was observed to be somewhat differently distributed in primary acini from Cel-MODY compared to the control and 16R mice. CEL-containing granules are normally located in the apical part of acinar cells, while zymogen granules in Cel-MODY are also found in the basolateral side. This altered intracellular distribution was also seen in immunostainings of pancreatic FFPE tissues sections

performed by others in the group. This finding is also consistent with what has previously been published; in chronic pancreatitis: it is often observed that the zymogen granules are present in a somewhat disorganized manner within the acinar cells (Bockman, 1997). Because we only studied 3-month old mice in this thesis, our observation would need to be further verified in mice that are older in age, where a worse phenotype is expected.

On the other hand, the distribution of the other tested markers (i.e., GM130, calnexin, BiP, and trypsin) in acini isolated from Cel-MODY, Cel-16R, and control mice were not markedly different. Surprisingly, our results did not show an increment in the ER stress marker for Cel-MODY mice compared to the two controls. Previous studies have shown that the CEL-MODY protein has an increased tendency to aggregate and induce ER-stress in cell lines (Gravdal et al., 2021; Johansson et al., 2011; Torsvik et al., 2009; Xiao et al., 2016). A reason for this could be sick and fragile cells may not survive the isolation. The immunostaining performed here is also a less quantitative method, and ER stress is likely to be better quantified and evaluated by performing real-time PCR or Western-Blot.

This experiment aimed to stain the various cellular organelles and CEL protein simultaneously. However, some of the antibodies needed different optimal conditions, and double staining with some of the markers proved difficult. For this reason and due to time constraints, only single stains were performed in this thesis. Trypsin and CEL have different protocols and did not work in the same conditions. The antibodies GM130, BiP, and Calnexin worked well alone but did not work together with CEL. Different conditions were tried such as guanidine hydrochloride, quenching with ammonium chloride (NH_4Cl), and antigen retrieval in citrate- and tris-based antigen unmasking solution. Other markers were also tried such as a commercially available CEL antibody from Sigma, Grp94 (ER), BiP antibodies from different companies (ER), GCNT1 (Golgi apparatus), different LAMP-1 and -2 antibodies (lysosome), amylase (zymogen granules), CHOP (ER-stress).

6.2.4 Assessing the secretory capacity of acinar cells

The function of pancreatic acinar cells is to produce and secrete digestive enzymes (Logsdon & Ji, 2013). The secretion can be evaluated by amylase secretion assay, which serves as a global measure for the secretory capacity. The secretion of digestive enzymes is primarily induced by hormonal or neuronal stimulation such as cholecystokinin (CCK), carbachol, and cerulein.

Direct imaging of secretion is also possible, allowing studies of the secretion at sub-cellular resolution (Geron et al., 2014).

Amylase secretion showed significant differences in Cel-MODY mice compared to control mice at low basal secretion (without stimulation of CCK-8). This could indicate that Cel-MODY acini have a lower basal secretion or there was less material in Cel-MODY mice. The acini were not responding to high concentrations of CCK-8 (10^{-6}, 10^{-7}, and 10^{-8} M), but responding to smaller concentrations of CCK-8 (10^{-11} and 10^{-10} M), which is consistent with findings in other studies (Williams, 2010; Xiao & Cui, 2004). The peak level of CCK-8 for all mice strains was 10^{-11} M, however, there was no significant differences observed between Cel-MODY mice and control mice. This correlates to a previous study where the peak level was between 10^{-10} to 10^{-11} M (Hampton et al., 1998). This correlates to the physiological concentrations and results in the highest amylase secretion (Liddle et al., 1988).

An important limitation of the study is that we have not been able to normalize the number of acini used in the experiment, as mentioned above. The data would also be improved by the present as percent amylase released of total amylase present in the cells. This could have been done by lysing the acini and measure the total amylase content inside the acini. The CCK hormone includes different fragments, and, in this study, we only used octapeptide, CCK-8 to stimulate the secretion, whereas it is the major transmitterform (Rehfeld et al., 2007).

6.3 Assessment of islet function

6.3.1 The islet isolation method

The function of pancreatic islets is to release hormones that plays a key role in the regulation of blood glucose (Carter et al., 2009). Pancreatic islets are essential in the pathophysiology of diabetes through β-cell failure to secrete enough insulin to regulate the blood glucose (Donath & Halban, 2004). Over the last few years, the interest in islet replacement therapies in humans has increased and contributed to methods used in isolating pancreatic islets from humans (Hogan et al., 2008). The isolated islets can be used for *in-vivo* transplantation and *in-vitro* studies, with a primary goal to obtain purified islets of Langerhans to respond similarly to the function *in-vivo*. In this thesis, the initial protocol of mouse islet isolation has been optimized after integrating elements from different published protocols.

Collagenase perfusion and digestion time

A critical step is successful perfusion for rapid and proper digestion necessary to obtain a high yield of high-quality islets. Collagenase perfusion through the ampulla of Vater allows the collagenase to traverse the anatomical structures of the organ. The perfusion reduces mechanical damage to the islets by less stirring or shaking, and the perfusion may also interact closely with connective tissues surrounding the islets. However, cannulation through the ampulla of Vater requires repeated practice and technical skills. There are also different commercial types of collagenase consisting of different components, and there is also variability in the activity that may cause fluctuation in the different batches.

Another important factor to obtain good quality and quantity of the islets is the digestion time. The digestion time was initially set to 13 min for all experiments, and different times were tried (9 min, 15 min, and 17 min). After some experience, quality and quantity variations were observed with 13 min digestion time. Therefore, every isolation required individual digestion time. Some training and experience are needed to decide optimal digestion time. In our experience, over-digestion results in lower islet yield, bad islet shape, reduced viability, and function. Under-digestion leads to reduced yield where the islets stick to the exocrine tissue and bad purity with more contaminations.

Separation and enrichment of pancreatic islets

Density gradient can be used to purity islets. McCall et al. compared different gradient components to find the optimal gradient for islet isolation (McCall et al., 2011). Based on the study obtained, we used Histopaque based on the recovery, viability, purity, and functionality *in-vitro* of islets.

After the density gradient separation, light microscopy was used to identify the islets of Langerhans followed by handpicking of those islets that looked healthy. To identify and recognize the islets, cells were stained with the zinc-binding substance diphenylthiocarbazone (DTZ). Stained islets with DTZ turn red in contrast to unstained acini and ductal cells. After some experience, the ability to recognize islets the procedure was performed without DTZ-staining.

Yield and recovery in growth media

The total number of islets from the pancreas varies significantly among strains and the age of the mouse (Carter et al., 2009). The technician skills, as well as the isolation method used, will also influence the total yield of islets. Our yield from the isolation of islets of Langerhans varied from unsuccessful isolations with no islets at all to successful isolations with 300 islets pr mouse. Other studies with different protocols demonstrated a possible isolation number between 180-350 islets pr mouse for the C57BL/6 mouse strain (Stull et al., 2012; Villarreal et al., 2019). Our experience was that the Cel-MODY mice resulted in the lowest yield of islets, compared to Cel-16R and the control mice. As mentioned above, the Cel-MODY mice have fat-replacement in the pancreas, and this could explain the lower yield in Cel-MODY mice. The islets may attach to the fat during the washing step and could be washed away together with the fat. This correlates with a similar observation done by Carter et al. where lean mice show tendencies to have higher purity and yield compared to mice with more fat (Carter et al., 2009). Another reason could also be that Cel-MODY mice have fewer islets than control mice.

The islets undergo tough processes during isolation by collagenase and mechanically shaking. To ensure the best recovery of isolated islets, the islets were incubated overnight to ensure their integrity in proper culture conditions before being employed in experiments. Different glucose concentrations might also play a role during the isolation and culturing of islets. RPMI was used as a culture medium with a glucose concentration of 11 mM. Other culture media as HBSS (5.5 mM) and DMEM (25 mM) was also tried but were unsuccessful. Medium containing 11 mM glucose has showed increased viability and lower apoptosis rates compared to media with both higher and lower glucose concentrations (Efanova et al., 1998).

6.3.2 Insulin secretion in response to extracellular glucose: GSIS assay

One of the main functions of pancreatic islets of Langerhans is to regulate insulin secretion in response to direct changes in the extracellular concentration of glucose (German, 1993). Our islets purified from the three mice strains did all recognize different extracellular glucose concentrations and secreted various levels of insulin based on the concentration of glucose.

Although there was no statistically significant difference, islets from Cel-16R seemed to have the highest capacity of insulin secretion. However, there was a significant difference in the secreted insulin levels between the three experiments, this might at least partly be explained by different sizes of islets. Large islets can develop hypoxic cells in their center, recognized as darker cells are more likely to undergo cell death and may lower secretion of insulin (Komatsu

et al., 2018). The challenges for this experiment were the variable yield of isolation, especially from Cel-MODY mice. Numerous mice might be needed if the isolation is unsuccessful and/or the yield is low.

7 Conclusions

The CEL-MODY syndrome is characterized by pancreatic exocrine dysfunction and subsequently develops diabetes. The main advantages of *ex-vivo* models are that the cells can be controlled and manipulated in a growth medium. In Cel-MODY mice, we found fat replacement in the exocrine tissues as early as 3-months of age, but the mice were normoglycemic and had normal body weight. In the isolated acini, the distribution of CEL protein was slightly different in acini isolated from Cel-MODY compared to two control mice strains. No marked differences were observed in distribution of various cellular organelles.

Previous protocols for isolating islets of Langerhans were optimized. However, isolated acini and islets purified from Cel-MODY mice resulted in lower amount of cellular material, in all isolations. This could possibly reflect only acini and islets from healthy and intact lobes of the pancreas surviving the isolation. The isolated islets secreted insulin according to extracellular glucose concentrations and isolated acini were able to secrete amylase by stimulation with CCK. There were no significant differences between the mice strains in insulin secretion. However, Cel-MODY mice had lower basal insulin secretion compared to control mice. In order to understand better the islet and acini function in the CEL-MODY mice, it would be interesting to study in mice older than 6-months, where a worse phenotype is expected due to the progressive nature of the disease.

8 Future perspectives

To obtain more knowledge about the pathogenic mechanism in CEL-MODY and to finalize and extend the investigations described in this thesis, it will be desirable to:

- Investigate apoptosis in primary acini use different techniques
- Further optimize double-staining of CEL together with various cellular organelles
- Quantify ER-stress by performing western blotting or real-time PCR
- Investigate the viability of isolated islets of Langerhans
- Investigate the intracellular distribution of insulin in freshly isolated islets
- Quantify data normalization of isolated acini used in cellular metabolism and amylase secretion assay
- Extend the experimental endpoint to 6- and 12-month old mice to investigate the functional pancreatic units when the phenotype is more severe

References

Abouakil, N., & Lombardo, D. (1989). Inhibition of human milk bile-salt-dependent lipase by boronic acids. Implication to the bile salts activator effect. *Biochim Biophys Acta*, *1004*(2), 215-220. https://doi.org/10.1016/0005-2760(89)90270-1

Abouakil, N., Mas, E., Bruneau, N., Benajiba, A., & Lombardo, D. (1993). Bile salt-dependent lipase biosynthesis in rat pancreatic AR 4-2 J cells. Essential requirement of N-linked oligosaccharide for secretion and expression of a fully active enzyme. *Journal of Biological Chemistry*, *268*(34), 25755-25763. https://doi.org/https://doi.org/10.1016/S0021-9258(19)74454-8

Aghdassi, A. A., Mayerle, J., Christochowitz, S., Weiss, F. U., Sendler, M., & Lerch, M. M. (2011). Animal models for investigating chronic pancreatitis. *Fibrogenesis & tissue repair*, *4*(1), 26-26. https://doi.org/10.1186/1755-1536-4-26

Ahmed Ali, U., Issa, Y., Hagenaars, J. C., Bakker, O. J., van Goor, H., Nieuwenhuijs, V. B., Bollen, T. L., van Ramshorst, B., Witteman, B. J., Brink, M. A., Schaapherder, A. F., Dejong, C. H., Spanier, B. W., Heisterkamp, J., van der Harst, E., van Eijck, C. H., Besselink, M. G., Gooszen, H. G., van Santvoort, H. C., & Boermeester, M. A. (2016). Risk of Recurrent Pancreatitis and Progression to Chronic Pancreatitis After a First Episode of Acute Pancreatitis. *Clin Gastroenterol Hepatol*, *14*(5), 738-746. https://doi.org/10.1016/j.cgh.2015.12.040

Alberts B, J. A., Lewis J, et al. (2002). The Endoplasmic Reticulum. In N. Y. G. Science (Ed.), *Molecular Biology of the Cell. 4th edition.* https://www.ncbi.nlm.nih.gov/books/NBK26841/

American Diabetes, A. (2010). Diagnosis and classification of diabetes mellitus. *Diabetes care*, *33 Suppl 1*(Suppl 1), S62-S69. https://doi.org/10.2337/dc10-S062

Anık, A., Çatlı, G., Abacı, A., & Böber, E. (2015). Maturity-onset diabetes of the young (MODY): an update. *J Pediatr Endocrinol Metab*, *28*(3-4), 251-263. https://doi.org/10.1515/jpem-2014-0384

Archer, H., Jura, N., Keller, J., Jacobson, M., & Bar-Sagi, D. (2006). A mouse model of hereditary pancreatitis generated by transgenic expression of R122H trypsinogen. *Gastroenterology*, *131*(6), 1844-1855. https://doi.org/10.1053/j.gastro.2006.09.049

Asmat, U., Abad, K., & Ismail, K. (2016). Diabetes mellitus and oxidative stress—A concise review. *Saudi Pharmaceutical Journal*, *24*(5), 547-553. https://doi.org/https://doi.org/10.1016/j.jsps.2015.03.013

Athwal, T., Huang, W., Mukherjee, R., Latawiec, D., Chvanov, M., Clarke, R., Smith, K., Campbell, F., Merriman, C., Criddle, D., Sutton, R., Neoptolemos, J., & Vlatković, N. (2014). Expression of human cationic trypsinogen (PRSS1) in murine acinar cells promotes pancreatitis and apoptotic cell death. *Cell Death & Disease*, *5*(4), e1165-e1165. https://doi.org/10.1038/cddis.2014.120

Atkinson, M. A., Eisenbarth, G. S., & Michels, A. W. (2014). Type 1 diabetes. *Lancet (London, England)*, *383*(9911), 69-82. https://doi.org/10.1016/S0140-6736(13)60591-7

Beckmann, J. S., Estivill, X., & Antonarakis, S. E. (2007). Copy number variants and genetic traits: closer to the resolution of phenotypic to genotypic variability. *Nature Reviews Genetics*, *8*(8), 639-646. https://doi.org/10.1038/nrg2149

Bengtsson-Ellmark, S. H., Nilsson, J., Orho-Melander, M., Dahlenborg, K., Groop, L., & Bjursell, G. (2004). Association between a polymorphism in the carboxyl ester lipase gene and serum cholesterol profile. *European Journal of Human Genetics*, *12*(8), 627-632. https://doi.org/10.1038/sj.ejhg.5201204

Beyer, G., Habtezion, A., Werner, J., Lerch, M. M., & Mayerle, J. (2020). Chronic pancreatitis. *The Lancet*, *396*(10249), 499-512. https://doi.org/10.1016/S0140-6736(20)31318-0

Bhatia, M., Wong, F. L., Cao, Y., Lau, H. Y., Huang, J., Puneet, P., & Chevali, L. (2005). Pathophysiology of Acute Pancreatitis. *Pancreatology*, *5*(2-3), 132-144. https://doi.org/10.1159/000085265

Bläckberg, L., & Hernell, O. (1983). Further characterization of the bile salt-stimulated lipase in human milk. *FEBS Letters*, *157*(2), 337-341. https://doi.org/https://doi.org/10.1016/0014-5793(83)80571-7

Bläckberg, L., Lombardo, D., Hernell, O., Guy, O., & Olivecrona, T. (1981). Bile salt-stimulated lipase in human milk and carboxyl ester hydrolase in pancreatic juice: Are they identical enzymes? *FEBS Letters*, *136*(2), 284-288. https://doi.org/https://doi.org/10.1016/0014-5793(81)80636-9

Bläuer, M., Sand, J., Nordback, I., & Laukkarinen, J. (2014). A novel 2-step culture model for long-term in vitro maintenance of human pancreatic acinar cells. *Pancreas*, *43*(5), 762-767. https://doi.org/10.1097/mpa.0000000000000105

Bockman, D. E. (1997). Morphology of the exocrine pancreas related to pancreatitis [https://doi.org/10.1002/(SICI)1097-0029(19970601)37:5/6<509::AID-JEMT13>3.0.CO;2-U]. *Microscopy Research and Technique*, *37*(5-6), 509-519. https://doi.org/https://doi.org/10.1002/(SICI)1097-0029(19970601)37:5/6<509::AID-JEMT13>3.0.CO;2-U

Brissova, M., Fowler, M. J., Nicholson, W. E., Chu, A., Hirshberg, B., Harlan, D. M., & Powers, A. C. (2005). Assessment of human pancreatic islet architecture and composition by laser scanning confocal microscopy. *J Histochem Cytochem*, *53*(9), 1087-1097. https://doi.org/10.1369/jhc.5C6684.2005

Broome, D. T., Pantalone, K. M., Kashyap, S. R., & Philipson, L. H. (2021). Approach to the Patient with MODY-Monogenic Diabetes. *J Clin Endocrinol Metab*, *106*(1), 237-250. https://doi.org/10.1210/clinem/dgaa710

Bruneau, N., Nganga, A., Fisher, E. A., & Lombardo, D. (1997). O-Glycosylation of C-terminal Tandem-repeated Sequences Regulates the Secretion of Rat Pancreatic Bile Salt-dependent Lipase*. *Journal of Biological Chemistry*, *272*(43), 27353-27361. https://doi.org/https://doi.org/10.1074/jbc.272.43.27353

Cabrera, O., Berman, D. M., Kenyon, N. S., Ricordi, C., Berggren, P. O., & Caicedo, A. (2006). The unique cytoarchitecture of human pancreatic islets has implications for islet cell function. *Proc Natl Acad Sci U S A*, *103*(7), 2334-2339. https://doi.org/10.1073/pnas.0510790103

Campbell, J. E., & Newgard, C. B. (2021). Mechanisms controlling pancreatic islet cell function in insulin secretion. *Nature Reviews Molecular Cell Biology*, *22*(2), 142-158. https://doi.org/10.1038/s41580-020-00317-7

Carter, J. D., Dula, S. B., Corbin, K. L., Wu, R., & Nunemaker, C. S. (2009). A practical guide to rodent islet isolation and assessment. *Biological procedures online*, *11*, 3-31. https://doi.org/10.1007/s12575-009-9021-0

Castiello, F., Heileman, K., & Tabrizian, M. (2015). Microfluidic perfusion systems for secretion fingerprint analysis of pancreatic islets: Applications, challenges and opportunities. *Lab Chip*, *16*. https://doi.org/10.1039/C5LC01046B

Chatterjee, S., Khunti, K., & Davies, M. J. (2017). Type 2 diabetes. *The Lancet*, *389*(10085), 2239-2251. https://doi.org/https://doi.org/10.1016/S0140-6736(17)30058-2

Colnaghi, R., Carpenter, G., Volker, M., & O'Driscoll, M. (2011). The consequences of structural genomic alterations in humans: Genomic Disorders, genomic instability and cancer. *Seminars in Cell & Developmental Biology*, *22*(8), 875-885. https://doi.org/https://doi.org/10.1016/j.semcdb.2011.07.010

Condic, M. L. (2014). Totipotency: what it is and what it is not. *Stem cells and development*, *23*(8), 796-812. https://doi.org/10.1089/scd.2013.0364

Cooper, G. M. (2000). The Golgi Apparatus. In S. Associates (Ed.), *The Cell: A Molecular Approach* (2nd edition ed.). https://www.ncbi.nlm.nih.gov/books/NBK9838/

Corbo, V., Tortora, G., & Scarpa, A. (2012). Molecular pathology of pancreatic cancer: from bench-to-bedside translation. *Current drug targets*, *13*(6), 744-752. https://doi.org/10.2174/138945012800564103

Da Silva Xavier, G. (2018). The Cells of the Islets of Langerhans. *Journal of clinical medicine*, *7*(3), 54. https://doi.org/10.3390/jcm7030054

DeFronzo, R. A., Ferrannini, E., Groop, L., Henry, R. R., Herman, W. H., Holst, J. J., Hu, F. B., Kahn, C. R., Raz, I., Shulman, G. I., Simonson, D. C., Testa, M. A., & Weiss, R. (2015). Type 2 diabetes mellitus. *Nature Reviews Disease Primers*, *1*(1), 15019. https://doi.org/10.1038/nrdp.2015.19

Donath, M. Y., & Halban, P. A. (2004). Decreased beta-cell mass in diabetes: significance, mechanisms and therapeutic implications. *Diabetologia*, *47*(3), 581-589. https://doi.org/10.1007/s00125-004-1336-4

Doyle, A., McGarry, M. P., Lee, N. A., & Lee, J. J. (2012). The construction of transgenic and gene knockout/knockin mouse models of human disease. *Transgenic research*, *21*(2), 327-349. https://doi.org/10.1007/s11248-011-9537-3

Eckardt, S., McLaughlin, K. J., & Willenbring, H. (2011). Mouse chimeras as a system to investigate development, cell and tissue function, disease mechanisms and organ regeneration. *Cell cycle (Georgetown, Tex.)*, *10*(13), 2091-2099. https://doi.org/10.4161/cc.10.13.16360

Efanova, I. B., Zaitsev, S. V., Zhivotovsky, B., Köhler, M., Efendić, S., Orrenius, S., & Berggren, P. O. (1998). Glucose and tolbutamide induce apoptosis in pancreatic beta-cells. A process dependent on intracellular Ca2+ concentration. *J Biol Chem*, *273*(50), 33501-33507. https://doi.org/10.1074/jbc.273.50.33501

El Jellas, K., Dusatkova, P., Molnes, J., Haldorsen, I., Tjora, E., Johansson, B. B., Fjeld, K., Johansson, S., Pr˙hov·, n., Groop, L., Nj¯lstad, P., & Molven, A. (2021). Independent mutational events in the hypervariable region of the carboxyl ester lipase gene: Identification of two new CEL-MODY families from Sweden and the Czech Republic. *Pancreatology*, *20*.

El Jellas, K., Johansson, B. B., Fjeld, K., Antonopoulos, A., Immervoll, H., Choi, M. H., Hoem, D., Lowe, M. E., Lombardo, D., Njølstad, P. R., Dell, A., Mas, E., Haslam, S. M., & Molven, A. (2018). The mucinous domain of pancreatic carboxyl-ester lipase (CEL) contains core 1/core 2 O-glycans that can be modified by ABO blood group determinants. *J Biol Chem*, *293*(50), 19476-19491. https://doi.org/10.1074/jbc.RA118.001934

Fajans, S. S., Bell, G. I., & Polonsky, K. S. (2001). Molecular mechanisms and clinical pathophysiology of maturity-onset diabetes of the young. *N Engl J Med*, *345*(13), 971-980. https://doi.org/10.1056/NEJMra002168

Firdous, P., Nissar, K., Ali, S., Ganai, B. A., Shabir, U., Hassan, T., & Masoodi, S. R. (2018). Genetic Testing of Maturity-Onset Diabetes of the Young Current Status and Future Perspectives. *Front Endocrinol (Lausanne)*, *9*, 253. https://doi.org/10.3389/fendo.2018.00253

Fjeld, K., Weiss, F. U., Lasher, D., Rosendahl, J., Chen, J.-M., Johansson, B. B., Kirsten, H., Ruffert, C., Masson, E., Steine, S. J., Bugert, P., Cnop, M., Grützmann, R., Mayerle, J., Mössner, J., Ringdal, M., Schulz, H.-U., Sendler, M., Simon, P., Sztromwasser, P., Torsvik, J., Scholz, M., Tjora, E., Férec, C., Witt, H., Lerch, M. M., Njølstad, P. R., Johansson, S., & Molven, A. (2015). A recombined allele of the lipase gene CEL and its pseudogene CELP confers susceptibility to chronic pancreatitis. *Nature Genetics*, *47*(5), 518-522. https://doi.org/10.1038/ng.3249

Frantz, E., Souza-Mello, V., & Mandarim-de-Lacerda, C. (2012). Pancreas: Anatomy, diseases and health implications. *Pancreas: Anatomy, Diseases and Health Implications*, 1-52.

Gaiser, S., Daniluk, J., Liu, Y., Tsou, L., Chu, J., Lee, W., Longnecker, D. S., Logsdon, C. D., & Ji, B. (2011). Intracellular activation of trypsinogen in transgenic mice induces acute but not chronic pancreatitis. *Gut*, *60*(10), 1379-1388. https://doi.org/10.1136/gut.2010.226175

Gale, E. A. (2005). Type 1 diabetes in the young: the harvest of sorrow goes on. *Diabetologia*, *48*(8), 1435-1438. https://doi.org/10.1007/s00125-005-1833-0

Gardner, D. S., & Tai, E. S. (2012). Clinical features and treatment of maturity onset diabetes of the young (MODY). *Diabetes, metabolic syndrome and obesity : targets and therapy*, *5*, 101-108. https://doi.org/10.2147/DMSO.S23353

Garrick, D., Fiering, S., Martin, D. I. K., & Whitelaw, E. (1998). Repeat-induced gene silencing in mammals. *Nature Genetics*, *18*(1), 56-59. https://doi.org/10.1038/ng0198-56

Gerich, J. E. (1988). Lilly lecture 1988. Glucose counterregulation and its impact on diabetes mellitus. *Diabetes*, *37*(12), 1608-1617. https://doi.org/10.2337/diab.37.12.1608

Gerich, J. E., & Campbell, P. J. (1988). Overview of counterregulation and its abnormalities in diabetes mellitus and other conditions. *Diabetes Metab Rev*, *4*(2), 93-111. https://doi.org/10.1002/dmr.5610040202

German, M. S. (1993). Glucose sensing in pancreatic islet beta cells: the key role of glucokinase and the glycolytic intermediates. *Proceedings of the National Academy of Sciences of the United States of America*, *90*(5), 1781-1785. https://doi.org/10.1073/pnas.90.5.1781

Geron, E., Schejter, E. D., & Shilo, B.-Z. (2014). Assessing the secretory capacity of pancreatic acinar cells. *Journal of visualized experiments : JoVE*(90), 51799. https://doi.org/10.3791/51799

Girgis, C., & Gunton, J. (2012). Pancreatic beta-cell failure in the pathogenesis of type 2 diabetes. In (pp. 87-104).

Gout, J., Pommier, R. M., Vincent, D. F., Kaniewski, B., Martel, S., Valcourt, U., & Bartholin, L. (2013). Isolation and culture of mouse primary pancreatic acinar cells. *Journal of visualized experiments : JoVE*(78), 50514. https://doi.org/10.3791/50514

Gravdal, A., Xiao, X., Cnop, M., El Jellas, K., Johansson, S., Njølstad, P. R., Lowe, M. E., Johansson, B. B., Molven, A., & Fjeld, K. (2021). The position of single-base deletions in the VNTR sequence of the carboxyl ester lipase (CEL) gene determines proteotoxicity. *Journal of Biological Chemistry*, 100661. https://doi.org/https://doi.org/10.1016/j.jbc.2021.100661

Hall, B., Limaye, A., & Kulkarni, A. B. (2009). Overview: generation of gene knockout mice. *Current protocols in cell biology*, *Chapter 19*, Unit-19.12.17. https://doi.org/10.1002/0471143030.cb1912s44

Hampton, L., Ladenheim, E., Akeson, M., Way, J., Weber, H., Sutliff, V., Jensen, R., Wine, L., Arnheiter, H., & Battey, J. (1998). Loss of bombesin-induced feeding suppression in gastrin-releasing peptide receptor-deficient mice. *Proceedings of the National Academy of Sciences of the United States of America*, *95*, 3188-3192. https://doi.org/10.1073/pnas.95.6.3188

Hatting, M., Tavares, C. D. J., Sharabi, K., Rines, A. K., & Puigserver, P. (2018). Insulin regulation of gluconeogenesis. *Annals of the New York Academy of Sciences*, *1411*(1), 21-35. https://doi.org/10.1111/nyas.13435

Hegyi, E., & Sahin-Tóth, M. (2017). Genetic Risk in Chronic Pancreatitis: The Trypsin-Dependent Pathway. *Digestive Diseases and Sciences*, *62*(7), 1692-1701. https://doi.org/10.1007/s10620-017-4601-3

Hernell, O., & Olivecrona, T. (1974). Human milk lipases II. Bile salt-stimulated lipase. *Biochimica et Biophysica Acta (BBA) - Lipids and Lipid Metabolism*, *369*(2), 234-244. https://doi.org/https://doi.org/10.1016/0005-2760(74)90254-9

Hogan, A., Pileggi, A., & Ricordi, C. (2008). Transplantation: current developments and future directions; the future of clinical islet transplantation as a cure for diabetes. *Front Biosci*, *13*, 1192-1205. https://doi.org/10.2741/2755

Hui, D. Y., & Howles, P. N. (2002). Carboxyl ester lipase. *Journal of Lipid Research*, *43*(12), 2017-2030. https://doi.org/https://doi.org/10.1194/jlr.R200013-JLR200

Hurles, M. E., & Lupski, J. R. (2006). Recombination Hotspots in Nonallelic Homologous Recombination. In J. R. Lupski & P. Stankiewicz (Eds.), *Genomic Disorders: The Genomic Basis of Disease* (pp. 341-355). Humana Press. https://doi.org/10.1007/978-1-59745-039-3_24

Hyun, J. J., & Lee, H. S. (2014). Experimental models of pancreatitis. *Clinical endoscopy*, *47*(3), 212-216. https://doi.org/10.5946/ce.2014.47.3.212

Ichii, H., Inverardi, L., Pileggi, A., Molano, R. D., Cabrera, O., Caicedo, A., Messinger, S., Kuroda, Y., Berggren, P. O., & Ricordi, C. (2005). A novel method for the assessment of cellular composition and beta-cell viability in human islet preparations. *Am J Transplant*, *5*(7), 1635-1645. https://doi.org/10.1111/j.1600-6143.2005.00913.x

Ionescu-Tirgoviste, C., Gagniuc, P. A., Gubceac, E., Mardare, L., Popescu, I., Dima, S., & Militaru, M. (2015). A 3D map of the islet routes throughout the healthy human pancreas. *Scientific Reports*, *5*(1), 14634. https://doi.org/10.1038/srep14634

Jancsó, Z., & Sahin-Tóth, M. (2020). Mutation That Promotes Activation of Trypsinogen Increases Severity of Secretagogue-Induced Pancreatitis in Mice. *Gastroenterology*, *158*(4), 1083-1094. https://doi.org/10.1053/j.gastro.2019.11.020

Johansson, Torsvik, J., Bjørkhaug, L., Vesterhus, M., Ragvin, A., Tjora, E., Fjeld, K., Hoem, D., Johansson, S., Ræder, H., Lindquist, S., Hernell, O., Cnop, M., Saraste, J., Flatmark, T., Molven, A., & Njølstad, P. R. (2011). Diabetes and pancreatic exocrine dysfunction due to mutations in the carboxyl ester lipase gene-maturity onset diabetes of the young (CEL-MODY): a protein misfolding disease. *J Biol Chem*, *286*(40), 34593-34605. https://doi.org/10.1074/jbc.M111.222679

Johansson, B. B., Fjeld, K., El Jellas, K., Gravdal, A., Dalva, M., Tjora, E., Ræder, H., Kulkarni, R. N., Johansson, S., Njølstad, P. R., & Molven, A. (2018). The role of the carboxyl ester lipase (CEL) gene in pancreatic disease. *Pancreatology*, *18*(1), 12-19. https://doi.org/10.1016/j.pan.2017.12.001

Kalra, S., & Gupta, Y. (2016). The Insulin:Glucagon Ratio and the Choice of Glucose-Lowering Drugs. *Diabetes therapy : research, treatment and education of diabetes and related disorders*, *7*(1), 1-9. https://doi.org/10.1007/s13300-016-0160-4

Kamisawa, T., Wood, L. D., Itoi, T., & Takaori, K. (2016). Pancreatic cancer. *The Lancet*, *388*(10039), 73-85. https://doi.org/https://doi.org/10.1016/S0140-6736(16)00141-0

Kim, A., Miller, K., Jo, J., Kilimnik, G., Wojcik, P., & Hara, M. (2009). Islet architecture: A comparative study. *Islets*, *1*(2), 129-136. https://doi.org/10.4161/isl.1.2.9480

Kim, J. W., Luo, J. Z. Q., & Luo, L. (2019). Chapter 10 - Bone Marrow Mesenchymal Stem Cells as a New Therapeutic Approach for Diabetes Mellitus. In X.-D. Chen (Ed.), *A Roadmap to Non-Hematopoietic Stem Cell-based Therapeutics* (pp. 251-273). Academic Press. https://doi.org/https://doi.org/10.1016/B978-0-12-811920-4.00010-0

Kirkegård, J., Mortensen, F. V., & Cronin-Fenton, D. (2017). Chronic Pancreatitis and Pancreatic Cancer Risk: A Systematic Review and Meta-analysis. *Am J Gastroenterol*, *112*(9), 1366-1372. https://doi.org/10.1038/ajg.2017.218

Kleeff, J., Whitcomb, D. C., Shimosegawa, T., Esposito, I., Lerch, M. M., Gress, T., Mayerle, J., Drewes, A. M., Rebours, V., Akisik, F., Muñoz, J. E. D., & Neoptolemos, J. P. (2017). Chronic pancreatitis. *Nature Reviews Disease Primers*, *3*(1), 17060. https://doi.org/10.1038/nrdp.2017.60

Kleinberger, J. W., Copeland, K. C., Gandica, R. G., Haymond, M. W., Levitsky, L. L., Linder, B., Shuldiner, A. R., Tollefsen, S., White, N. H., & Pollin, T. I. (2018). Monogenic diabetes in overweight and obese youth diagnosed with type 2 diabetes: the TODAY clinical trial. *Genetics in Medicine*, *20*(6), 583-590. https://doi.org/10.1038/gim.2017.150

Komatsu, H., Kandeel, F., & Mullen, Y. (2018). Impact of Oxygen on Pancreatic Islet Survival. *Pancreas*, *47*(5), 533-543. https://doi.org/10.1097/MPA.0000000000001050

Lambert, R. (1965). Surgery of the Digestive System in the Rat. In.

Lampel, M., & Kern, H. F. (1977). Acute interstitial pancreatitis in the rat induced by excessive doses of a pancreatic secretagogue. *Virchows Arch A Pathol Anat Histol*, *373*(2), 97-117. https://doi.org/10.1007/bf00432156

Ledermann, B. (2000). Embryonic stem cells and gene targeting. *Exp Physiol*, *85*(6), 603-613.

Lee, M. G., Kim, J. W., Kim, K. H., & Muallen, S. (2002). Molecular mechanism of pancreatic bicarbonate secretion. *Korean Journal of Physiology and Pharmacology*, *6*, 131-138.

Lee, P. J., & Papachristou, G. I. (2019). New insights into acute pancreatitis. *Nature Reviews Gastroenterology & Hepatology*, *16*(8), 479-496. https://doi.org/10.1038/s41575-019-0158-2

Lerch, M. M., & Gorelick, F. S. (2013). Models of Acute and Chronic Pancreatitis. *Gastroenterology*, *144*(6), 1180-1193. https://doi.org/10.1053/j.gastro.2012.12.043

Leslie, R. D. (2010). Predicting adult-onset autoimmune diabetes: clarity from complexity. *Diabetes*, *59*(2), 330-331. https://doi.org/10.2337/db09-1620

Leung, P. S., & Ip, S. P. (2006). Pancreatic acinar cell: its role in acute pancreatitis. *Int J Biochem Cell Biol*, *38*(7), 1024-1030. https://doi.org/10.1016/j.biocel.2005.12.001

Levy, J. (2009). Chapter 5 - Pulmonary Manifestations of Gastrointestinal Diseases. In N. L. Turcios & R. J. Fink (Eds.), *Pulmonary Manifestations of Pediatric Diseases* (pp. 98-120). W.B. Saunders. https://doi.org/https://doi.org/10.1016/B978-1-4160-3031-7.00005-X

Li, X., & Heyer, W.-D. (2008). Homologous recombination in DNA repair and DNA damage tolerance. *Cell Research*, *18*(1), 99-113. https://doi.org/10.1038/cr.2008.1

Lidberg, U., Nilsson, J., Stro¨mberg, K., Stenman, G. r., Sahlin, P., Enerba¨ck, S., & Bjursell, G. (1992). Genomic organization, sequence analysis, and chromosomal localization of the human car□yl ester lipase (CEL) gene and a CEL-like (CELL) gene. *Genomics*, *13*(3), 630-640. https://doi.org/https://doi.org/10.1016/0888-7543(92)90134-E

Liddle, R. A., Rushakoff, R. J., Morita, E. T., Beccaria, L., Carter, J. D., & Goldfine, I. D. (1988). Physiological role for cholecystokinin in reducing postprandial hyperglycemia in humans. *The Journal of clinical investigation*, *81*(6), 1675-1681. https://doi.org/10.1172/jci113505

Logsdon, C. D., & Ji, B. (2013). The role of protein synthesis and digestive enzymes in acinar cell injury. *Nature reviews. Gastroenterology & hepatology*, *10*(6), 362-370. https://doi.org/10.1038/nrgastro.2013.36

Logsdon, C. D., & Williams, J. A. (1986). Pancreatic acinar cells in monolayer culture: direct trophic effects of caerulein in vitro. *Am J Physiol*, *250*(4 Pt 1), G440-447. https://doi.org/10.1152/ajpgi.1986.250.4.G440

Lombardo, Guy, O., & Figarella, C. (1978). Purification and characterization of a carboxyl ester hydrolase from human pancreatic juice. *Biochimica et Biophysica Acta (BBA) - Enzymology*, *527*(1), 142-149. https://doi.org/https://doi.org/10.1016/0005-2744(78)90263-2

Lombardo, D., & Guy, O. (1980). Studies on the substrate specificity of a carboxyl ester hydrolase from human pancreatic juice. II. Action on cholesterol esters and lipid-soluble vitamin esters. *Biochimica et Biophysica Acta (BBA) - Enzymology*, *611*(1), 147-155. https://doi.org/https://doi.org/10.1016/0005-2744(80)90050-9

Longnecker, D. (2014). Anatomy and Histology of the Pancreas.

Loomes, K. M., Senior, H. E., West, P. M., & Roberton, A. M. (1999). Functional protective role for mucin glycosylated repetitive domains. *Eur J Biochem*, *266*(1), 105-111. https://doi.org/10.1046/j.1432-1327.1999.00824.x

Madeyski, K., Lidberg, U., Bjursell, G., & Nilsson, J. (1998). Structure and organization of the human carboxyl ester lipase locus. *Mamm Genome*, *9*(4), 334-338. https://doi.org/10.1007/s003359900762

Magnusson, I., Rothman, D. L., Katz, L. D., Shulman, R. G., & Shulman, G. I. (1992). Increased rate of gluconeogenesis in type II diabetes mellitus. A 13C nuclear magnetic resonance study. *The Journal of clinical investigation*, *90*(4), 1323-1327. https://doi.org/10.1172/jci115997

Maritim, A. C., Sanders, R. A., & Watkins, J. B., 3rd. (2003). Diabetes, oxidative stress, and antioxidants: a review. *J Biochem Mol Toxicol*, *17*(1), 24-38. https://doi.org/10.1002/jbt.10058

McCall, M. D., Maciver, A. H., Pawlick, R. L., Edgar, R., & Shapiro, A. M. J. (2011). Histopaque provides optimal mouse islet purification kinetics: Comparison study with Ficoll, iodixanol and dextran. *Islets*, *3*(4), 144-149. https://doi.org/10.4161/isl.3.4.15729

Mederos, M. A., Reber, H. A., & Girgis, M. D. (2021). Acute Pancreatitis: A Review. *JAMA*, *325*(4), 382-390. https://doi.org/10.1001/jama.2020.20317

Mitchell, P. (2012). *AO/PI Viability*. Retrieved 20.03 from https://www.nexcelom.com/aopi-viability/

Murphy, B. D. (2018). Mammalian Gestational Strategies: Embryonic Diapause and Pseudopregnancy. In M. K. Skinner (Ed.), *Encyclopedia of Reproduction (Second Edition)* (pp. 376-382). Academic Press. https://doi.org/https://doi.org/10.1016/B978-0-12-801238-3.64657-3

Narasimhan, V. M., Xue, Y., & Tyler-Smith, C. (2016). Human Knockout Carriers: Dead, Diseased, Healthy, or Improved? *Trends in Molecular Medicine*, *22*(4), 341-351. https://doi.org/https://doi.org/10.1016/j.molmed.2016.02.006

Neuschwander-Tetri, B. A., Bridle, K. R., Wells, L. D., Marcu, M., & Ramm, G. A. (2000). Repetitive Acute Pancreatic Injury in the Mouse Induces Procollagen α1(I) Expression Colocalized to Pancreatic Stellate Cells. *Laboratory Investigation*, *80*(2), 143-150. https://doi.org/10.1038/labinvest.3780018

Nilsson, J., Hellquist, M., & Bjursell, G. (1993). The Human Carboxyl Ester Lipase-like (CELL) Gene Is Ubiquitously Expressed and Contains a Hypervariable Region. *Genomics*, *17*(2), 416-422. https://doi.org/https://doi.org/10.1006/geno.1993.1341

Nkonge, K. M., Nkonge, D. K., & Nkonge, T. N. (2020). The epidemiology, molecular pathogenesis, diagnosis, and treatment of maturity-onset diabetes of the young (MODY). *Clinical Diabetes and Endocrinology*, *6*(1), 20. https://doi.org/10.1186/s40842-020-00112-5

Oliveira, S. C., Neves, J. S., Pérez, A., & Carvalho, D. (2020). Maturity-onset diabetes of the young: From a molecular basis perspective toward the clinical phenotype and proper management. *Endocrinol Diabetes Nutr*, *67*(2), 137-147. https://doi.org/10.1016/j.endinu.2019.07.012

Orci, L., Baetens, D., Ravazzola, M., Stefan, Y., & Malaisse-Lagae, F. (1976). Pancreatic polypeptide and glucagon : non-random distribution in pancreatic islets. *Life Sci*, *19*(12), 1811-1815. https://doi.org/10.1016/0024-3205(76)90112-0

Pandiri, A. R. (2014). Overview of exocrine pancreatic pathobiology. *Toxicologic pathology*, *42*(1), 207-216. https://doi.org/10.1177/0192623313509907

Parks, M. M., Lawrence, C. E., & Raphael, B. J. (2015). Detecting non-allelic homologous recombination from high-throughput sequencing data. *Genome Biology*, *16*(1), 72. https://doi.org/10.1186/s13059-015-0633-1

Pasqualini, E., Caillol, N., Valette, A., Lloubes, R., Verine, A., & Lombardo, D. (2000). Phosphorylation of the rat pancreatic bile-salt-dependent lipase by casein kinase II is essential for secretion. *The Biochemical journal*, *345 Pt 1*(Pt 1), 121-128. https://pubmed.ncbi.nlm.nih.gov/10600647
https://www.ncbi.nlm.nih.gov/pmc/articles/PMC1220738/
Peixoto-Barbosa, R., Reis, A. F., & Giuffrida, F. M. A. (2020). Update on clinical screening of maturity-onset diabetes of the young (MODY). *Diabetology & Metabolic Syndrome*, *12*(1), 50. https://doi.org/10.1186/s13098-020-00557-9
Pellegrini, S., Pipitone, G. B., Cospito, A., Manenti, F., Poggi, G., Lombardo, M. T., Nano, R., Martino, G., Ferrari, M., Carrera, P., Sordi, V., & Piemonti, L. (2021). Generation of β Cells from iPSC of a MODY8 Patient with a Novel Mutation in the Carboxyl Ester Lipase (CEL) Gene. *The Journal of Clinical Endocrinology & Metabolism*. https://doi.org/10.1210/clinem/dgaa986
Porta, M., Fabregat, X., Malats, N., Guarner, L., Carrato, A., de Miguel, A., Ruiz, L., Jariod, M., Costafreda, S., Coll, S., Alguacil, J., Corominas, J. M., Solà, R., Salas, A., & Real, F. X. (2005). Exocrine pancreatic cancer: symptoms at presentation and their relation to tumour site and stage. *Clin Transl Oncol*, *7*(5), 189-197. https://doi.org/10.1007/bf02712816
Rahib, L., Smith, B. D., Aizenberg, R., Rosenzweig, A. B., Fleshman, J. M., & Matrisian, L. M. (2014). Projecting cancer incidence and deaths to 2030: the unexpected burden of thyroid, liver, and pancreas cancers in the United States. *Cancer Res*, *74*(11), 2913-2921. https://doi.org/10.1158/0008-5472.Can-14-0155
Rawla, P., Sunkara, T., & Gaduputi, V. (2019). Epidemiology of Pancreatic Cancer: Global Trends, Etiology and Risk Factors. *World journal of oncology*, *10*(1), 10-27. https://doi.org/10.14740/wjon1166
Raz, A., & Perouansky, M. (2019). 8 - Central Nervous System Physiology: Neurophysiology. In H. C. Hemmings & T. D. Egan (Eds.), *Pharmacology and Physiology for Anesthesia (Second Edition)* (pp. 145-173). Elsevier. https://doi.org/https://doi.org/10.1016/B978-0-323-48110-6.00008-9
Rehfeld, J. F., Friis-Hansen, L., Goetze, J. P., & Hansen, T. V. (2007). The biology of cholecystokinin and gastrin peptides. *Curr Top Med Chem*, *7*(12), 1154-1165. https://doi.org/10.2174/156802607780960483
Reisner, H. M. (2014). Chapter 11: Pathology of the Pancreas. In Lange (Ed.), *Pathology: A Modern Case Study*.
Rodriguez-Diaz, R., Molano, R. D., Weitz, J. R., Abdulreda, M. H., Berman, D. M., Leibiger, B., Leibiger, I. B., Kenyon, N. S., Ricordi, C., Pileggi, A., Caicedo, A., & Berggren, P.-O. (2018). Paracrine Interactions within the Pancreatic Islet Determine the Glycemic Set Point. *Cell metabolism*, *27*(3), 549-558.e544. https://doi.org/10.1016/j.cmet.2018.01.015
Rogers, S., Wells, R., & Rechsteiner, M. (1986). Amino acid sequences common to rapidly degraded proteins: the PEST hypothesis. *Science*, *234*(4774), 364-368. https://doi.org/10.1126/science.2876518
Rosenthal, K. L., & Wyre, N. R. (2012). Chapter 7 - Endocrine Diseases. In K. E. Quesenberry & J. W. Carpenter (Eds.), *Ferrets, Rabbits, and Rodents (Third Edition)* (pp. 86-102). W.B. Saunders. https://doi.org/https://doi.org/10.1016/B978-1-4160-6621-7.00007-5
Roxvall, L., Bengtson, A., Sennerby, L., & Heideman, M. (1991). Activation of the complement cascade by trypsin. *Biol Chem Hoppe Seyler*, *372*(4), 273-278. https://doi.org/10.1515/bchm3.1991.372.1.273
Ræder, H., Haldorsen, I. S., Ersland, L., Grüner, R., Taxt, T., Søvik, O., Molven, A., & Njølstad, P. R. (2007). Pancreatic Lipomatosis Is a Structural Marker in Nondiabetic Children With Mutations in Carboxyl-Ester Lipase. *Diabetes*, *56*(2), 444. https://doi.org/10.2337/db06-0859
Ræder, H., Johansson, S., Holm, P. I., Haldorsen, I. S., Mas, E., Sbarra, V., Nermoen, I., Eide, S. Å., Grevle, L., Bjørkhaug, L., Sagen, J. V., Aksnes, L., Søvik, O., Lombardo, D., Molven, A., & Njølstad, P. R. (2006). Mutations in the CEL VNTR cause a syndrome of diabetes and pancreatic exocrine dysfunction. *Nature Genetics*, *38*(1), 54-62. https://doi.org/10.1038/ng1708
Ræder, H., McAllister, F. E., Tjora, E., Bhatt, S., Haldorsen, I., Hu, J., Willems, S. M., Vesterhus, M., El Ouaamari, A., Liu, M., Ræder, M. B., Immervoll, H., Hoem, D., Dimcevski, G., Njølstad, P. R., Molven, A., Gygi, S. P., & Kulkarni, R. N. (2014). Carboxyl-ester lipase maturity-onset diabetes of the young is associated with development of pancreatic cysts and upregulated

MAPK signaling in secretin-stimulated duodenal fluid. *Diabetes*, *63*(1), 259-269. https://doi.org/10.2337/db13-1012

Ræder, H., Vesterhus, M., El Ouaamari, A., Paulo, J. A., McAllister, F. E., Liew, C. W., Hu, J., Kawamori, D., Molven, A., Gygi, S. P., Njølstad, P. R., Kahn, C. R., & Kulkarni, R. N. (2013). Absence of diabetes and pancreatic exocrine dysfunction in a transgenic model of carboxyl-ester lipase-MODY (maturity-onset diabetes of the young). *PloS one*, *8*(4), e60229-e60229. https://doi.org/10.1371/journal.pone.0060229

Saluja, A., Saito, I., Saluja, M., Houlihan, M. J., Powers, R. E., Meldolesi, J., & Steer, M. (1985). In vivo rat pancreatic acinar cell function during supramaximal stimulation with caerulein. *Am J Physiol*, *249*(6 Pt 1), G702-710. https://doi.org/10.1152/ajpgi.1985.249.6.G702

Sarantis, P., Koustas, E., Papadimitropoulou, A., Papavassiliou, A. G., & Karamouzis, M. V. (2020). Pancreatic ductal adenocarcinoma: Treatment hurdles, tumor microenvironment and immunotherapy. *World journal of gastrointestinal oncology*, *12*(2), 173-181. https://doi.org/10.4251/wjgo.v12.i2.173

Siegel, R., Ma, J., Zou, Z., & Jemal, A. (2014). Cancer statistics, 2014. *CA Cancer J Clin*, *64*(1), 9-29. https://doi.org/10.3322/caac.21208

Slack, J. M. (1995). Developmental biology of the pancreas. *Development*, *121*(6), 1569-1580.

Smith, M. E., & Morton, D. G. (2010). *The digestive system : basic science and clinical conditions* (2nd ed. ed.). Churchill Livingstone Elsevier.

Steiner, D. J., Kim, A., Miller, K., & Hara, M. (2010). Pancreatic islet plasticity: interspecies comparison of islet architecture and composition. *Islets*, *2*(3), 135-145. https://doi.org/10.4161/isl.2.3.11815

Stull, N. D., Breite, A., McCarthy, R., Tersey, S. A., & Mirmira, R. G. (2012). Mouse islet of Langerhans isolation using a combination of purified collagenase and neutral protease. *Journal of visualized experiments : JoVE*(67), 4137. https://doi.org/10.3791/4137

Taylor, A. K., Zambaux, J. L., Klisak, I., Mohandas, T., Sparkes, R. S., Schotz, M. C., & Lusis, A. J. (1991). Carboxyl ester lipase: A highly polymorphic locus on human chromosome 9qter. *Genomics*, *10*(2), 425-431. https://doi.org/https://doi.org/10.1016/0888-7543(91)90328-C

Thorens, B. (2011). Brain glucose sensing and neural regulation of insulin and glucagon secretion. *Diabetes Obes Metab*, *13 Suppl 1*, 82-88. https://doi.org/10.1111/j.1463-1326.2011.01453.x

Tjora, E., Wathle, G., Engjom, T., Erchinger, F., Molven, A., Aksnes, L., Haldorsen, I. S., Dimcevski, G., Njølstad, P. R., & Ræder, H. (2013). Severe Pancreatic Dysfunction But Compensated Nutritional Status in Monogenic Pancreatic Disease Caused by Carboxyl-Ester Lipase Mutations. *Pancreas*, *42*(7). https://journals.lww.com/pancreasjournal/Fulltext/2013/10000/Severe_Pancreatic_Dysfunction_But_Compensated.5.aspx

Torsvik, J., Johansson, B. B., Dalva, M., Marie, M., Fjeld, K., Johansson, S., Bjørkøy, G., Saraste, J., Njølstad, P. R., & Molven, A. (2014). Endocytosis of secreted carboxyl ester lipase in a syndrome of diabetes and pancreatic exocrine dysfunction. *The Journal of biological chemistry*, *289*(42), 29097-29111. https://doi.org/10.1074/jbc.M114.574244

Torsvik, J., Johansson, S., Johansen, A., Ek, J., Minton, J., Ræder, H., Ellard, S., Hattersley, A., Pedersen, O., Hansen, T., Molven, A., & Njølstad, P. R. (2009). Mutations in the VNTR of the carboxyl-ester lipase gene (CEL) are a rare cause of monogenic diabetes. *Human Genetics*, *127*(1), 55. https://doi.org/10.1007/s00439-009-0740-8

Uehara, S., Honjyo, K., Furukawa, S., Hirayama, A., & Sakamoto, W. (1989). Role of the kallikrein-kinin system in human pancreatitis. *Adv Exp Med Biol*, *247b*, 643-648. https://doi.org/10.1007/978-1-4615-9546-5_106

Urakami, T. (2019). Maturity-onset diabetes of the young (MODY): current perspectives on diagnosis and treatment. *Diabetes, metabolic syndrome and obesity : targets and therapy*, *12*, 1047-1056. https://doi.org/10.2147/dmso.S179793

Vaxillaire, M., Boccio, V., Philippi, A., Vigouroux, C., Terwilliger, J., Passa, P., Beckmann, J. S., Velho, G., Lathrop, G. M., & Froguel, P. (1995). A gene for maturity onset diabetes of the young (MODY) maps to chromosome 12q. *Nature Genetics*, *9*(4), 418-423. https://doi.org/10.1038/ng0495-418

Vesterhus, M., Ræder, H., Kurpad, A. J., Kawamori, D., Molven, A., Kulkarni, R. N., Ronald Kahn, C., & Rasmus Njølstad, P. (2010). Pancreatic Function in Carboxyl-Ester Lipase Knockout Mice. *Pancreatology*, *10*(4), 467-476. https://doi.org/https://doi.org/10.1159/000266284

Villarreal, D., Pradhan, G., Wu, C. S., Allred, C. D., Guo, S., & Sun, Y. (2019). A Simple High Efficiency Protocol for Pancreatic Islet Isolation from Mice. *J Vis Exp*(150). https://doi.org/10.3791/57048

Whitcomb, D. C., & Lowe, M. E. (2007). Human Pancreatic Digestive Enzymes. *Digestive Diseases and Sciences*, *52*(1), 1-17. https://doi.org/10.1007/s10620-006-9589-z

Whitcomb, D. C., & Lowe, M. E. (2007). Human pancreatic digestive enzymes. *Dig Dis Sci*, *52*(1), 1-17. https://doi.org/10.1007/s10620-006-9589-z

Williams, J. A. (2001). Intracellular signaling mechanisms activated by cholecystokinin-regulating synthesis and secretion of digestive enzymes in pancreatic acinar cells. *Annu Rev Physiol*, *63*, 77-97. https://doi.org/10.1146/annurev.physiol.63.1.77

Williams, J. A. (2010). Isolation of rodent pancreatic acinar cells and acini by collagenase digestion.

Williams, J. A., Korc, M., & Dormer, R. L. (1978). Action of secretagogues on a new preparation of functionally intact, isolated pancreatic acini. *Am J Physiol*, *235*(5), 517-524. https://doi.org/10.1152/ajpendo.1978.235.5.E517

Williams, J. A., Sans, M. D., Tashiro, M., Schäfer, C., Bragado, M. J., & Dabrowski, A. (2002). Cholecystokinin activates a variety of intracellular signal transduction mechanisms in rodent pancreatic acinar cells. *Pharmacol Toxicol*, *91*(6), 297-303. https://doi.org/10.1034/j.1600-0773.2002.910606.x

Wäsle, B., & Edwardson, J. M. (2002). The regulation of exocytosis in the pancreatic acinar cell. *Cell Signal*, *14*(3), 191-197. https://doi.org/10.1016/s0898-6568(01)00257-1

Xiao, R., & Cui, Z. J. (2004). Mutual dependence of VIP/PACAP and CCK receptor signaling for a physiological role in duck exocrine pancreatic secretion. *American journal of physiology. Regulatory, integrative and comparative physiology*, *286*, R189-198. https://doi.org/10.1152/ajpregu.00265.2003

Xiao, X., Jones, G., Sevilla, W. A., Stolz, D. B., Magee, K. E., Haughney, M., Mukherjee, A., Wang, Y., & Lowe, M. E. (2016). A Carboxyl Ester Lipase (CEL) Mutant Causes Chronic Pancreatitis by Forming Intracellular Aggregates That Activate Apoptosis. *J Biol Chem*, *291*(44), 23224-23236. https://doi.org/10.1074/jbc.M116.734384

Xu, D., & Esko, J. D. (2009). A Golgi-on-a-chip for glycan synthesis. *Nature Chemical Biology*, *5*(9), 612-613. https://doi.org/10.1038/nchembio0909-612

Yamamoto, M., Otani, M., & Otsuki, M. (2006). A new model of chronic pancreatitis in rats. *Am J Physiol Gastrointest Liver Physiol*, *291*(4), G700-708. https://doi.org/10.1152/ajpgi.00502.2005

Zeng, M., Vachel, L., & Muallem, S. (2018). Physiology of Duct Cell Secretion: An Integrated Textbook of Basic Science, Medicine, and Surgery. In (pp. 78-90). https://doi.org/10.1002/9781119188421.ch5

Zhang, X., & Wang, Y. (2016). Glycosylation Quality Control by the Golgi Structure. *Journal of molecular biology*, *428*(16), 3183-3193. https://doi.org/10.1016/j.jmb.2016.02.030

Zhou, B., Lu, Y., Hajifathalian, K., Bentham, J., & Di Cesare, M. (2016). Worldwide trends in diabetes since 1980: a pooled analysis of 751 population-based studies with 4·4 million participants. *The Lancet*, *387*(10027), 1513-1530. https://doi.org/10.1016/S0140-6736(16)00618-8